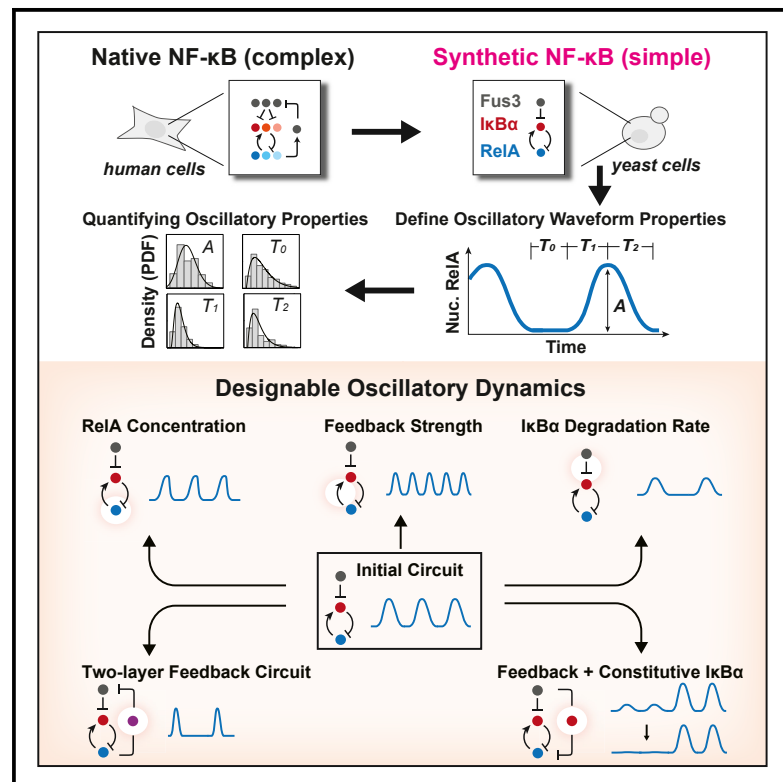


Design of Tunable Oscillatory Dynamics in a Synthetic NF- κ B Signaling Circuit

Graphical Abstract



Authors

Zhi-Bo Zhang, Qiu-Yue Wang,
Yu-Xi Ke, ..., Wendell A. Lim,
Chao Tang, Ping Wei

Correspondence

pwei@pku.edu.cn

In Brief

The design principles of oscillatory signaling behaviors were explored through synthetically engineering NF- κ B circuit in combination with mathematical modeling.

Highlights

- Engineering robustly oscillating synthetic NF- κ B circuit in yeast
- Predictable oscillatory waveforms by tuning circuit parameters
- Frequency-only modulation enabled by two-layer feedbacks
- Accurate design of custom oscillatory signaling behaviors

Design of Tunable Oscillatory Dynamics in a Synthetic NF- κ B Signaling Circuit

Zhi-Bo Zhang,^{1,2} Qiu-Yue Wang,¹ Yu-Xi Ke,³ Shi-Yu Liu,² Jian-Qi Ju,^{1,2} Wendell A. Lim,^{4,5} Chao Tang,¹ and Ping Wei^{1,2,6,*}

¹Center for Quantitative Biology and Peking-Tsinghua Joint Center for Life Sciences, Academy for Advanced Interdisciplinary Studies, Peking University, Beijing 100871, China

²The MOE Key Laboratory of Cell Proliferation and Differentiation, School of Life Sciences, Peking University, Beijing 100871, China

³School of Life Sciences, Tsinghua University, Beijing 100084, China

⁴Center for Systems and Synthetic Biology, Department of Cellular and Molecular Pharmacology, University of California, San Francisco, San Francisco, CA 94158, USA

⁵Howard Hughes Medical Institute, University of California, San Francisco, San Francisco, CA 94158, USA

⁶Lead Contact

*Correspondence: pwei@pku.edu.cn

<https://doi.org/10.1016/j.cels.2017.09.016>

SUMMARY

Although oscillatory circuits are prevalent in transcriptional regulation, it is unclear how a circuit's structure and the specific parameters that describe its components determine the shape of its oscillations. Here, we engineer a minimal, inducible human nuclear factor κ B (NF- κ B)-based system that is composed of NF- κ B (RelA) and degradable inhibitor of NF- κ B ($I\kappa$ B α), into the yeast, *Saccharomyces cerevisiae*. We define an oscillation's waveform quantitatively as a function of signal amplitude, rest time, rise time, and decay time; by systematically tuning RelA concentration, the strength of negative feedback, and the degradation rate of $I\kappa$ B α , we demonstrate that peak shape and frequency of oscillations can be controlled *in vivo* and predicted mathematically. In addition, we show that nested negative feedback loops can be employed to specifically tune the frequency of oscillations while leaving their peak shape unchanged. In total, this work establishes design principles that enable function-guided design of oscillatory signaling controllers in diverse synthetic biology applications.

INTRODUCTION

Oscillatory signals control many important biological functions, including cell cycle (Ferrell et al., 2011; Tyson, 1991), circadian rhythms (Partch et al., 2014), and vertebrate somitogenesis (Oates et al., 2012). The design principles of natural and synthetic oscillators have been studied extensively, such as the regulation of periodicity (Elowitz and Leibler, 2000; Hess and Boiteux, 1971; Novák and Tyson, 2008), robustness (Potvin-Trottier et al., 2016; Stricker et al., 2008; Tsai et al., 2008), and entrainment (Hasty et al., 2002; Mondragon-Palmino et al., 2011). More recently, it has been found that eukaryotic cells could encode information in the quantitatively different temporal

behaviors of Msn2 in yeast and p53 in mammals (Behar and Hoffmann, 2010; Levine et al., 2013). Remarkably, such quantitative signaling dynamics were often oscillatory or pulsatile. The particular properties of oscillatory signaling dynamics (e.g., amplitude, frequency) have shown great benefit to coordinate (Cai et al., 2008) or differentially regulate gene expression (Werner et al., 2005; Ashall et al., 2009; Hao et al., 2013; Purvis et al., 2012) in stress signaling and inflammatory response. It remains incompletely understood how the properties of such oscillatory dynamics are controlled in natural systems and how they could be tailored synthetically.

The NF- κ B in immune response is one of the well-known signaling systems to be highly dynamic, responding to various extracellular antigens or cytokines. Notably, the fluorescence-tagged NF- κ B protein (i.e., RelA) was found to be activated in a damped oscillatory fashion in response to tumor necrosis factor α (TNF- α) (Nelson et al., 2004; Tay et al., 2010). The core design of the circuit underlying this oscillator is similar to that of many biological oscillators; a negative feedback loop with time delay, usually consisting of a transcription factor (i.e., NF- κ B) and an inhibitory protein (i.e., $I\kappa$ B). The oscillatory cycles involve the following reactions: the degradation of $I\kappa$ B (e.g., $I\kappa$ B α , $I\kappa$ B β , and $I\kappa$ B ϵ) releases the inhibition of NF- κ B (e.g., RelA, RelB, cRelA, p50, and p52) (Hayden and Ghosh, 2008), leading to the production of new $I\kappa$ B, which in turn inhibits the transcriptional activity of NF- κ B, thereby completing the cycle (Figure 1A) (Hoffmann et al., 2002; Nelson et al., 2004). However, in practice, because the native NF- κ B system exists in the complicated context of mammalian cells, it is difficult to specifically experimentally probe and rewire the circuit components of such oscillatory signaling networks.

To surpass such limitations, we sought to rationally design and build a synthetic oscillatory signaling circuit by recapitulating a human NF- κ B module (i.e., $I\kappa$ B α -RelA protein complex). Our design emphasized orthogonality and predictable tuning performances. Here, we describe an engineered circuit contains a synthetic promoter module that can program oscillatory dynamics of NF- κ B at the transcriptional level, and also a synthetic phospho-degron module that allows programming at the post-translational level. We implement the circuit in *S. cerevisiae* and demonstrate that the peak shape and the period of the

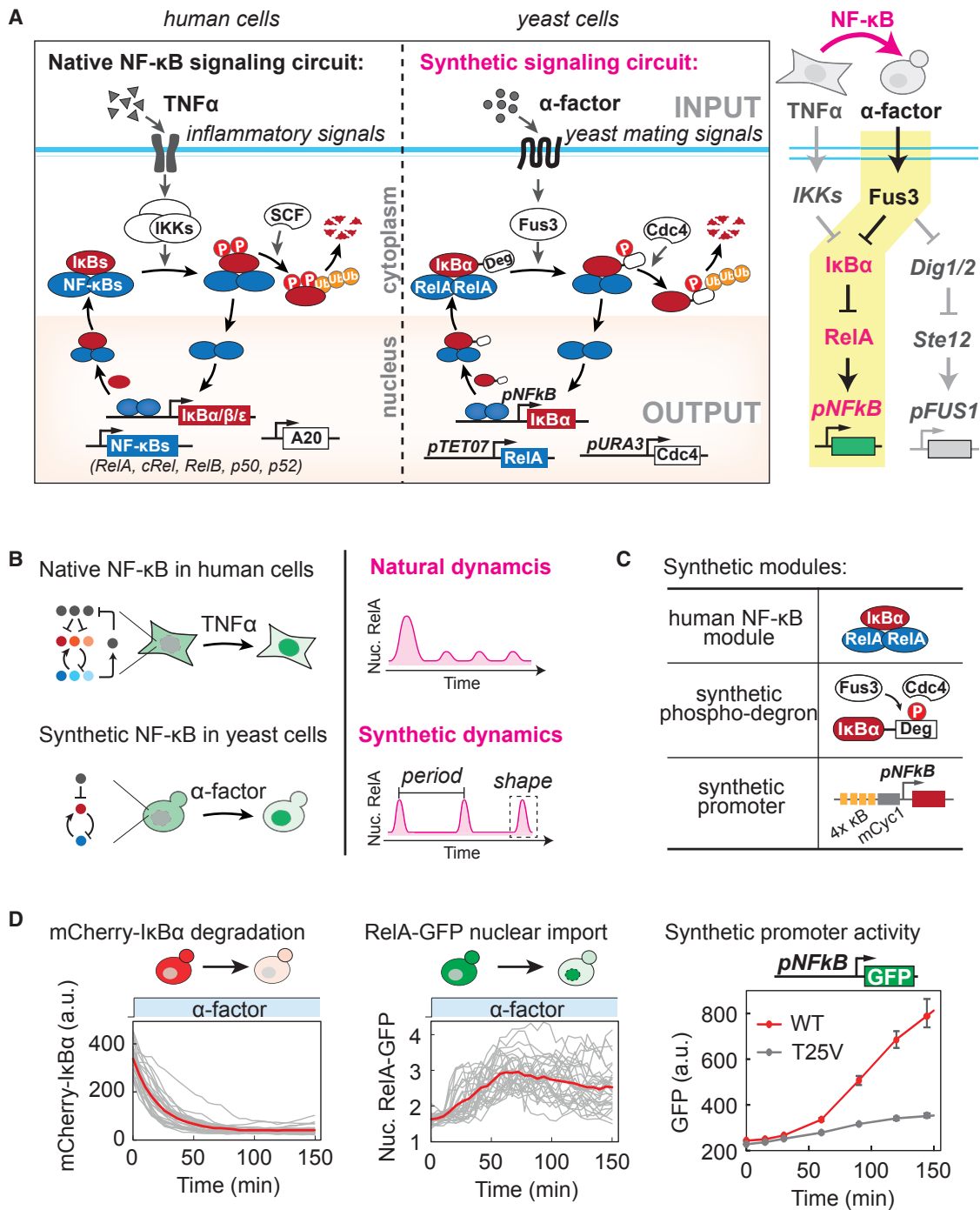


Figure 1. Design of Synthetic Oscillatory NF- κ B Circuit in Yeast Cells

(A) Schematic of the native and synthetic NF- κ B signaling circuits. The downstream module of human NF- κ B pathway, I κ B α -RelA, is rewired to the downstream of the yeast mating MAPK pathway.

(B) In contrast to the complex native NF- κ B system in mammalian cells (damped oscillation upon TNF- α stimulation), the synthetic signaling circuit can be precisely designed to generate novel oscillatory waveforms with the specific period (or frequency) and peak shape, due to the simplified and well-defined circuit structures and parameters. The time courses of RelA nuclear localization in yeast cells were measured to monitor the activation dynamics of the system.

(C) The synthetic oscillatory signaling circuit was based on three synthetic modules: the human I κ B α -RelA protein complex as the core circuit module; a synthetic degron module that enables the phosphorylation-dependent degradation of the engineered I κ B α , allowing the activation of the synthetic circuits by yeast mating pheromone (α factor); an NF- κ B-responsive synthetic promoter module that enables the feedback-driven activation of I κ B α expression.

(legend continued on next page)

oscillatory waveforms could be tuned using a combination of three parameters: protein level of RelA, negative feedback strength, and the protein stability of I κ B α . Incorporating a second negative feedback loop between RelA and the upstream kinase Fus3 enabled frequency-only tuning of oscillatory waveforms. Our work demonstrates a proof-of-concept for the design of cellular circuits that use built-in modules to respond to diverse input signals and to dynamic cellular information (Behar and Hoffmann, 2010; Purvis and Lahav, 2013).

RESULTS

Design of Synthetic NF- κ B Signaling Circuit in Yeast Cells

To investigate how the design of circuits influences their outputs (i.e., oscillatory dynamics), we built a synthetic oscillatory signaling circuit in yeast by recapitulating the I κ B α -RelA module from the human NF- κ B system. Given that they completely lack the human NF- κ B system (Gilmore and Wolenski, 2012), yeast cells provide a homologous but orthogonal cellular environment for investigating a streamlined form of the refabricated NF- κ B circuit and for designing customized signaling outputs with engineered dynamics (Kachroo et al., 2015) (Figure 1B). To achieve tunable levels of RelA protein, we used a doxycycline-inducible promoter (*pTET07*) to drive the expression of RelA-GFP in a titratable manner. To implement this oscillator in yeast, we had to engineer another two control modules that allowed the integration of the circuit into the endogenous signaling and transcriptional machinery of yeast (Figure 1C). First, we engineered a phosphorylation-regulated degron module to achieve post-translational control over the degradation of the inhibitor protein I κ B α that tagged with the synthetic degron. This process completely mimicked the activation mechanism in the native NF- κ B system (Figure 1A). The synthetic degron can be phosphorylated by the activated yeast mating mitogen-activated protein kinase (MAPK) Fus3, resulting in the recognition by the cytosolic Cdc4 tagged with a nuclear export signal peptide (Figure S1B), which normally functions as an E3 ligase in the yeast nucleus (Gordley et al., 2016). Accordingly, the I κ B α protein is degraded rapidly upon treatment with the yeast mating pheromone, α factor, allowing the RelA to translocate to the nucleus and activate the downstream gene transcription. Second, to implement the transcriptional control of I κ B α by RelA, we engineered a synthetic yeast-compatible NF- κ B-responsive promoter module (incorporating a minimal yeast CYC1 promoter with four tandem repeats of NF- κ B binding sites) to drive the expression of I κ B α (Figure 1C). We found that these components in the human NF- κ B module functioned as designed in yeast cells: RelA formed a protein complex with I κ B α and remained in the cytoplasm; free RelA was localized in the nucleus (Figure S1A); adding α factor triggered activation of the degradation of I κ B α and released RelA into the nucleus to activate the expression of GFP reporter (Figure 1D). Having established that we can use RelA to regulate I κ B α transcription, we assumed

that the newly synthesized I κ B α would bind with nuclear RelA, retain RelA in the cytoplasm, thereby generating an effective time-delayed negative feedback loop (Figure 1A).

Synthetic NF- κ B Circuit Generated Robust Oscillatory Dynamics in Response to Continuous Stimulation of the Yeast Mating Pheromone

To test our design, we monitored yeast cells containing the synthetic signaling circuit at single-cell resolution. To maintain a consistent α factor concentration, we used a microfluidic device to replenish the supply of α factor over time, and employed time-lapse microscopy to track the RelA-GFP localization dynamics. We observed that the addition of α factor triggered the periodic shuttling of RelA-GFP between the nucleus and the cytoplasm (Figure 2A; Movie S1). Long-term (10 hr) monitoring of the nuclear RelA-GFP dynamics revealed a robust oscillatory pattern (Figures 2B and S2); more than 80% of cells exhibited this pattern of oscillation (Figure S3, total $n = 60$). We also found RelA was weakly activated in a spontaneous oscillatory pattern, even in the absence of α factor (Figure S2). We rationalized this observation as follows: the cycle of degradation and re-synthesis of I κ B α was likely still happening in a weak manner without input signals, considering that the I κ B α expression was fully dependent on the activated RelA.

Characterizing the Waveform Properties of the Oscillatory Dynamics

To more precisely evaluate the characteristics of the oscillatory dynamics generated by our synthetic signaling circuit, we defined four properties of an oscillatory waveform: the peak amplitude (A) and three individual time segments, including the rest time (T_0), the rise time (T_1), and the decay time (T_2). Together, these four properties are adequate to define the period and the peak shape of any oscillatory waveforms (Figure 2C) (McClung, 2008). Using the data from our initial single-cell experiments, we calculated that the oscillation had a mean amplitude of 3.5 (a.u.) and an oscillation period of 100 min ($T_0 = 44$ min, $T_1 = 26$ min, and $T_2 = 30$ min) (Figure 2D). This period in our initial design is very close to that of the natural NF- κ B oscillation in mammalian cells (Hoffmann et al., 2002; Nelson et al., 2004; Tay et al., 2010). Despite this similarity in periodicity, our synthetic oscillatory signaling circuit exhibited a more sustained pattern of oscillation than what has been previously reported for the native NF- κ B system, which has a severely damped oscillation pattern following TNF- α stimulus (Hoffmann et al., 2002; Nelson et al., 2004; Tay et al., 2010).

Parameter Tuning in the Initial Circuit Leads to Predictable Waveform Changes

The simplicity of our synthetic system allowed us to further fine-tune the behavior of our oscillatory circuit. To explore the relationship between the properties of oscillatory waveforms and the parameters of the synthetic circuit, we sequentially tuned

(D) Mating pheromone-activated signaling modules in the synthetic NF- κ B circuit. mCherry-I κ B α degradation and RelA-GFP nuclear import (Nuc.:Tot. ratio) were recorded in single-cell time-lapse imaging (gray). The mean was calculated by over 50 cells (red). The transcriptional activity was measured from *pNF κ B*-driven GFP expression. Average GFP fluorescence of yeast strains with wild-type degron (red) or mutated inactive degron (T25V, gray) with SD measured from triplicated experiments.

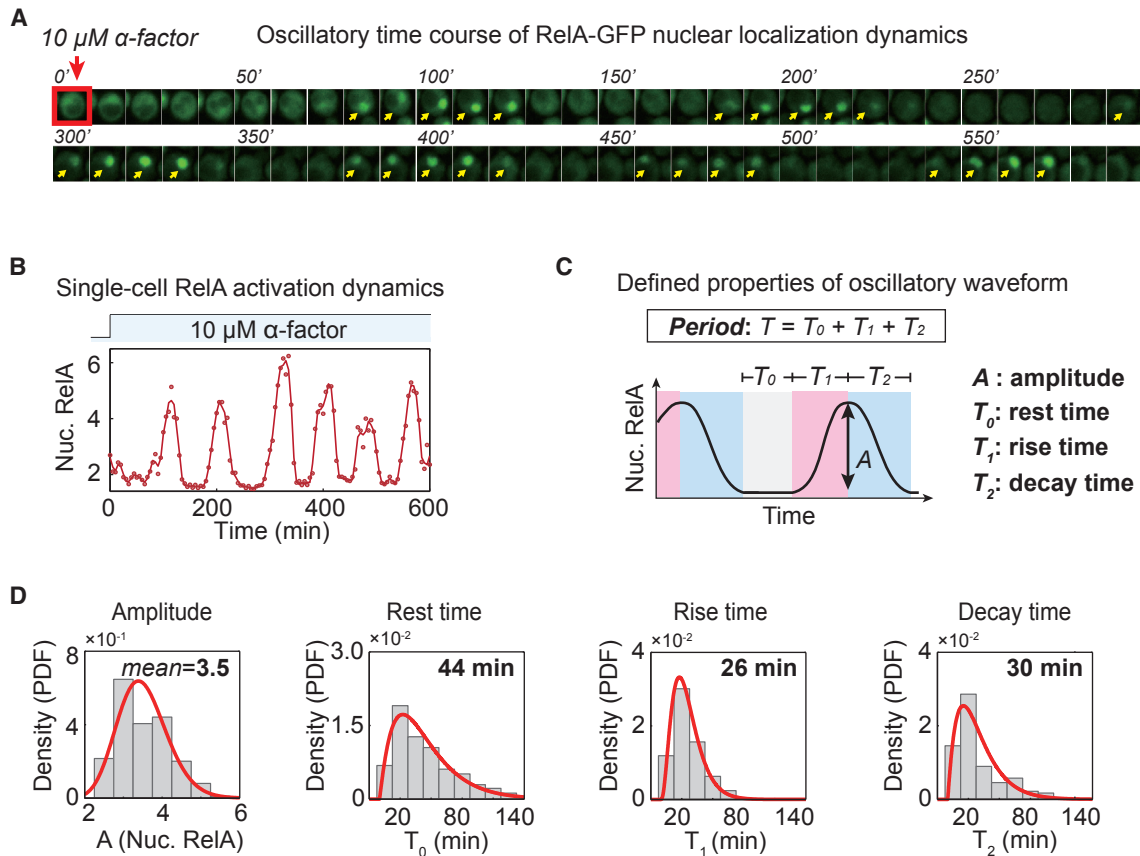


Figure 2. Characterization of Oscillatory Waveform Generated by Synthetic Signaling Circuit

(A) RelA-GFP nuclear localization traces were recorded by continuously monitoring yeast cells engineered with the synthetic oscillatory signaling circuit. After the addition of α factor ($10 \mu\text{M}$), RelA-GFP shuttled in and out of the nucleus (yellow arrows) in an oscillatory fashion.

(B) RelA-GFP nuclear localization dynamics were quantified from time-lapse fluorescent images in (A). The raw data are shown in dots; the line was smoothed by Savitzky-Golay filter.

(C) The oscillatory waveform could be defined as the combination of the four independent properties: rest time, T_0 ; the rise time, T_1 ; the decay time, T_2 ; and A , amplitude.

(D) The distribution and mean values for the four oscillatory properties were calculated from at least 50 cells. The probability density function (PDF, red) was obtained by fitting a gamma distribution to the experimental data.

the following parameters: the protein concentration of RelA (α), the strength of the negative feedback loop (β), and the degradation rate of $\text{IkB}\alpha$ (γ) (Figures 3A–3C). We used a range of doxycycline concentrations (from 0.5 to 5 $\mu\text{g}/\text{mL}$) to tune the RelA protein concentration, and obtained up to a 5-fold change in the RelA level (Figure 3A). Tuning down the RelA protein level resulted in a short period (high frequency) (Figure 3D; Movie S2). The negative feedback strength (β) was tuned by a set of variant synthetic promoters with graded activities to drive $\text{IkB}\alpha$ expression (Figure 3B). The strong feedback strength resulted in a high frequency oscillation (Figure 3E; Movie S3). The $\text{IkB}\alpha$ degradation rate (γ) was then tuned by introducing a series of single amino acid mutations into the synthetic degron (Figure 3C). The slow degradation of $\text{IkB}\alpha$ resulted in a slow frequency oscillation (Figure 3F; Movie S4). The single-cell oscillatory dynamics from each parameter-tuning clearly exhibited diverse peak shapes as well as frequencies (Figures 3D–3F and S4A).

To analyze the quantitative changes of oscillatory waveforms, we quantified the tuned waveforms using the aforementioned

properties, T_0 , T_1 , T_2 , and A (Figure 2C), and compared them between each tuning. The tuning of each of the three circuit parameters resulted in changes in particular properties of the waveform. More specifically, tuning down the RelA protein concentration resulted in both a faster decay and a lower amplitude (a peak shape with less symmetry); increasing the negative feedback strength resulted in faster rise and decay; and decreasing the $\text{IkB}\alpha$ degradation rate resulted in both longer rest times and lower amplitudes (Figures 3D–3F and S4B). To better understand our parameter-tuning results, we then constructed a mathematical model to systematically explore the relationship between the waveform properties and circuit parameters (Figures 4A–4C). Our simulation presented similar parameter-tuning results as our experimental data (Figure 4D). Together, these results demonstrated that, guided by a predictive model, we could selectively tune a particular combination of parameters in synthetic circuits and generate oscillatory waveforms with target frequency or peak shape. Note that our modeling demonstrates that a circuit incorporated with key components as our three synthetic modules allowed us to

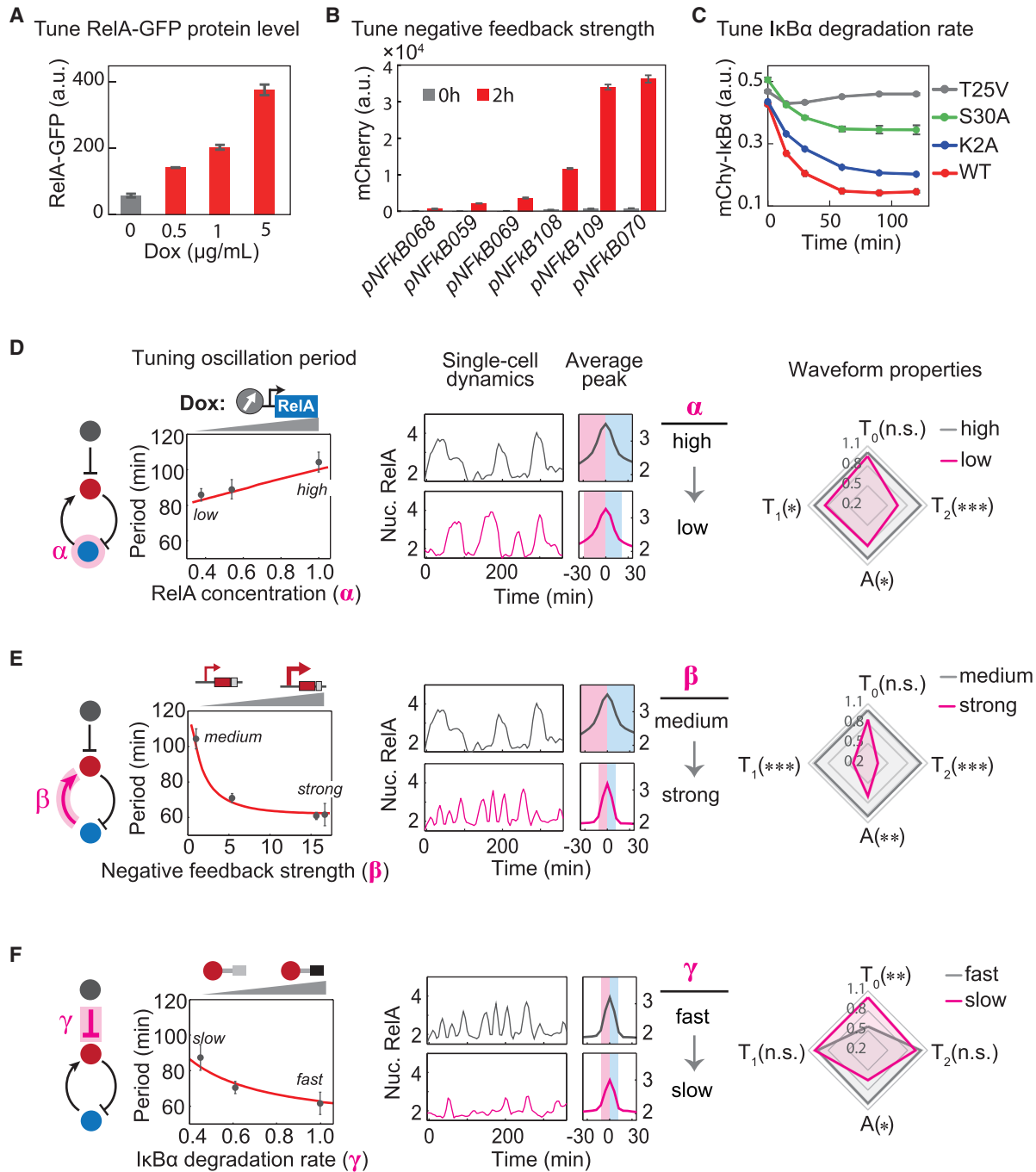


Figure 3. Parameter Tuning in the Synthetic Oscillatory Circuit

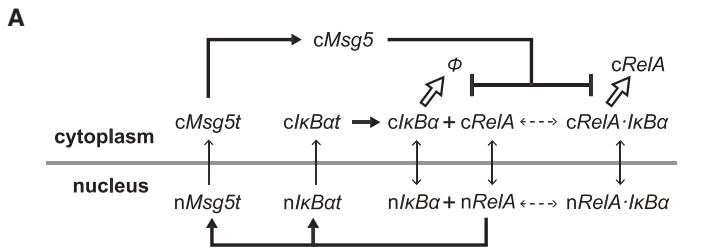
(A) The protein level of RelA-GFP was tuned by varying doses of doxycycline. The expression of RelA-GFP was driven by a synthetic doxycycline-inducible promoter *pTET07*. RelA-GFP level was measured after a 12-hr treatment of doxycycline. The error bars were calculated from the SD of triplicate experiments.

(B) The feedback strength was tuned by incorporating a series of synthetic NF-κB promoters with gradient transcriptional activities. The promoter activity was indicated by the fluorescent density of mCherry with 2-hr induction of RelA in absence of IκBα. The error bars were calculated from the SD of triplicate experiments.

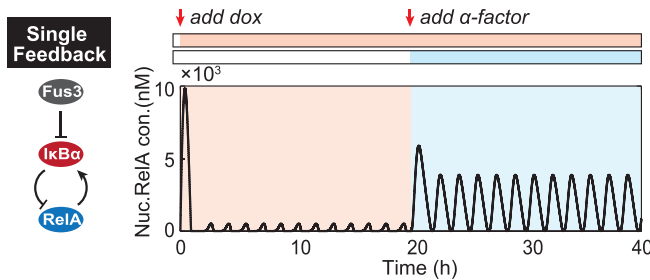
(C) The IκBα degradation rate was tuned by introducing single amino acid mutation in the synthetic degen. The time courses of the decay of mCherry-tagged IκBα were measured by flow cytometry after treatment with 10 μM α factor at time zero.

(D) Tuning the RelA-GFP protein level (α). The measured period values of the synthetic circuit are plotted as gray circles, with error bars indicating the SD from at least three independent experiments. The red line represents our model prediction. Single-cell dynamics obtained from high to low RelA concentration are shown in the middle panel. The rise phase (pink shadow) and decay phase (blue shadow) are highlighted in the peaks averaged from at least 50 cells. The Radar chart shows relative changes of four properties (T_0 , T_1 , T_2 , and A , defined in Figure 2C) when tuning of oscillatory waveforms by varying RelA concentration (for each

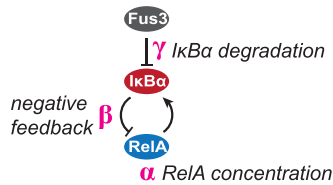
(legend continued on next page)



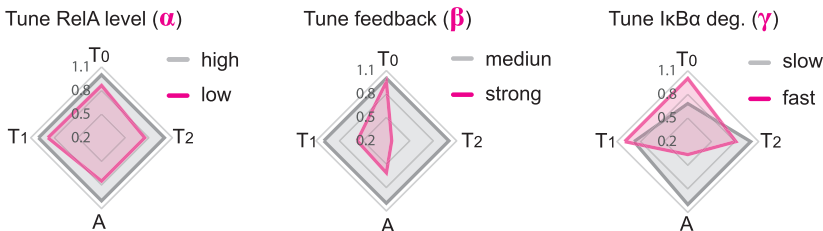
B Model simulation of RelA activation dynamics of the synthetic circuit



C Tunable circuit parameters:



D Model-predicted waveform properties by tuning circuit parameters



tune the waveform at both transcriptional and post-translational level.

Circuit Structure with Two-Layer Negative Feedback Loops Enables Frequency-Only Tuning of Oscillatory Waveforms

The preceding experiments focused on the tuning of individual parameters in a circuit that contained a single negative feedback loop. However, the circuit architectures of naturally evolved oscillators are typically more complicated, often

Figure 4. Mathematical Modeling and Prediction of Signaling Behaviors of Synthetic Circuits

(A) Diagram of the dynamic model for the synthetic signaling circuit. Solid thin arrows indicate molecular nuclear translocation. Dashed arrows indicate the formation and deformation of protein complex. Thick arrows represent the process of transcription or translation, and thick bar lines represent the inhibitory effect of Msg5 on the degradation of lκBα. (B) Simulated RelA activation dynamics in the initial circuit (with one single negative feedback loop). Doxycycline (5 μg/mL) was added at t = 0, 10 μM α factor was added at t = 20 hr.

(C) Tuning parameters in each synthetic module: α, the total concentration of RelA protein; β, the strength of the negative feedback loop; and γ, the rate of lκBα degradation.

(D) The predicted waveform properties (T_0 , T_1 , T_2 , and A) when tuning α, β, and γ in the model simulation agreed with our experimental observations in Figure 3. The maximum value of each property was normalized as “1.”

consisting of multiple layers of regulations. For instance, the human NF-κB has feedback regulators comprised of other lκBs (e.g., lκBε) and also other layers of negative feedback regulators, such as A20, which regulate the upstream nodes, lκB kinases (Hayden and Ghosh, 2008; Werner et al., 2008). The multi-layer negative feedback loops, a topology referred to as “nested negative feedback loops” (Mengel et al., 2012), facilitate complex regulation of the NF-κB dynamics. We speculated that we might be able to recapitulate this topology design of nested negative feedback loops to produce unique effects on the oscillatory waveforms. To explore this idea, we computationally simulated the output behaviors of a circuit that included a second negative feedback loop. Our simulations

of the oscillatory behaviors of this circuit showed that the addition of a second negative feedback loop in another layer (to form the nested negative feedback loops) contributes specifically to the lengthening of the rest time T_0 , without affecting other properties of the oscillatory waveform. In contrast, when adding a second negative feedback in parallel, both the period and the peak shape of the waveform were altered (Figure 5A). In other words, this design of two-layer negative feedback loops enables a unique mode of waveform-tuning, with which we could specifically tune the frequency while maintaining the peak shape (changes are only in the rest time).

chart, the maximum value measured for each of the properties was set to 1). The significance of the difference between conditions was assessed with two-sample Student's t tests (n.s., not significant; *p < 0.05; **p < 0.01; ***p < 0.001).

(E) Tune the negative feedback strength (β).

(F) Tune the degradation rate of lκBα (γ).

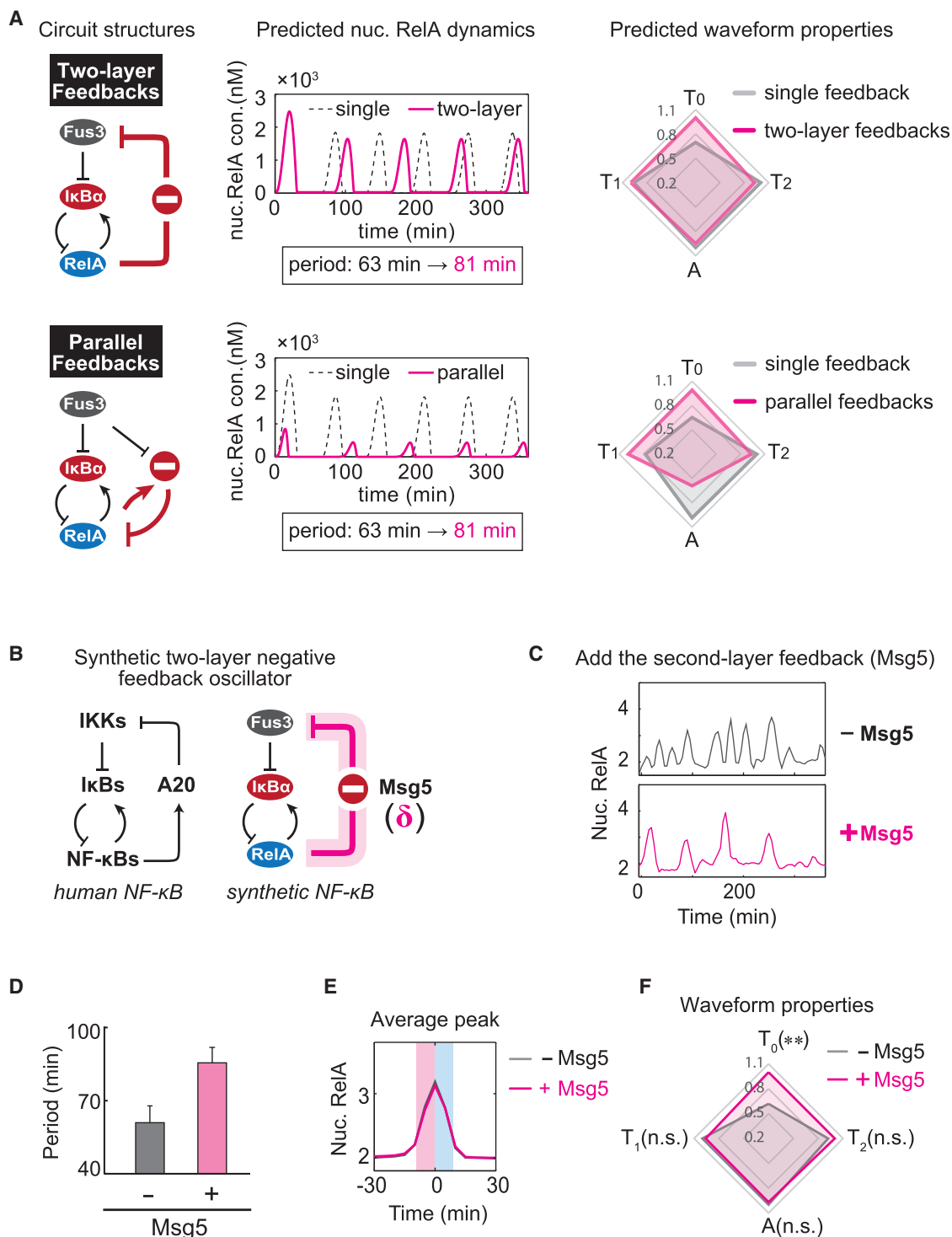


Figure 5. Circuit Structure with Two-Layer Negative Feedback Loops Enables Frequency-Only Tuning of Oscillatory Waveforms

(A) Model prediction of RelA activation dynamics and waveform properties when adding a second negative feedback in two different ways: two-layer feedbacks (upper panel) or parallel feedbacks (lower panel). The periods of two types of dual-feedback circuit were set as equal (81 min). The modeling results showed that the circuit structure with two-layer feedbacks maintained the peak shape (only T_0 was changed); the circuit structure with parallel feedbacks changed multiple waveform properties (T_0 , T_1 , and A).

(B) Simplified diagram of the circuit structure with two-layer negative feedback loops in comparison with the human NF- κ B system. The second layer of feedback was engineered using the RelA-dependent expression of a yeast MAPK phosphatase Msg5, which can dephosphorylate Fus3. The parameter δ represents the strength of the negative feedback loop mediated by Msg5.

(C) Representative single-cell analysis of the synthetic oscillatory signaling circuit with (pink) and without (gray) feedback mediated by Msg5.

(legend continued on next page)

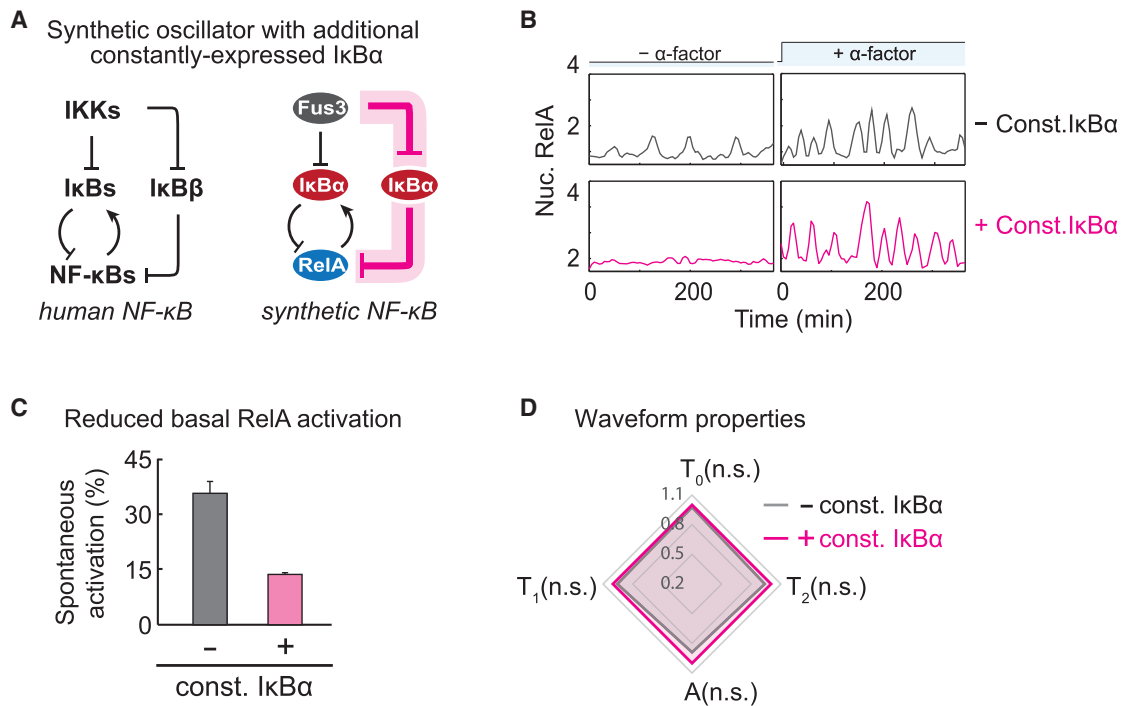


Figure 6. Circuit Structure with Both Feedback-Expressed and Constantly Expressed IκBα Reduced the Spontaneous RelA Activation

(A) Diagram of the circuit structure with additional constantly expressed IκBα in comparison with the human NF-κB system. In addition to the feedback-expressed IκBα, the second copy of IκBα was expressed from a continuously active promoter, *pURA3*. (B) Single-cell analysis of the synthetic oscillatory signaling circuit with (pink) and without (gray) constantly expressed IκBα, before or after adding 10 μM α factor. (C) Statistical analysis of the spontaneously activated cells before adding 10 μM α factor. The spontaneous activation was calculated from the percentage of activated cell. A cell, in which RelA nuclear translocation shows at least one detectable peak within a 6 hr-observation window without α factor stimulation, was considered as the activated cell. The error bars were calculated from the SD of at least three independent experiments. (D) The waveform properties showed no evident changes by adding constantly expressed IκBα. n.s., not significant.

To test the model prediction, we experimentally engineered a circuit with two-layer negative feedback loops by incorporating the yeast MAPK phosphatase *Msg5*, which can effectively repress the upstream kinase *Fus3* (Bashor et al., 2008) (Figure S5A), under the control of a synthetic NF-κB promoter (Figure 5B). As predicted, the oscillatory waveform generated by the circuit with the two-layer loops extended the period by specifically elongating the T_0 while maintaining the peak shape of the waveform (Figures 5C–5F; Movie S5). In other words, the RelA activation dynamics show a similar pulsatile waveform across a wide range of tuned frequencies. In addition, we demonstrated that the rest time could be gradually increased by enhancing the strength of the second feedback loop (Figures S5B and S5C).

Circuit Structure with Additional Constantly Expressed IκBα Prevented Basal RelA Activation

Within the native, mammalian system, some portion of IκBs (i.e., IκBβ) are constantly expressed and independent of NF-κB activation in the natural NF-κB system. These constantly expressed

IκBs were suggested to cause the damping effect in response to TNF-α, and knocking out IκBβ resulted in more robust oscillation of RelA nuclear occupancy (Hoffmann et al., 2002). Therefore, we asked whether a similar effect could be observed in our synthetic oscillatory circuit. To answer this question, we introduced another copy of IκBα with the same degron, while driven by a constitutive yeast promoter *pURA3*, into our initial design of oscillatory circuit (with a single negative feedback loop) (Figure 6A). Contrary to our expectation given the observations of the native system, neither the peak shape nor the period were changed within our engineered circuit. All four waveform properties remained the same (Figures 6B and 6D). However, when we looked at the cells before adding α factor, we found the basal level of RelA activation (the spontaneously activated RelA without α factor stimulation, see also Figure S2) were significantly reduced (Figures 6B and 6C). When we further tuned the protein level of this constant IκBα, we observed that the spontaneous RelA activation could be continuously decreased by increasing the level of the constant IκBα (Figures S6A–S6D). When the constant IκBα was expressed in relatively high level,

(D) Periods of the synthetic oscillatory signaling circuit with and without the *Msg5* loop. The error bars were calculated from the SD of at least three independent experiments. (E) The average peaks from oscillations with (pink line) or without (gray line) *Msg5* loop were almost identical (rise time, pink shadow; decay time, blue shadow). (F) The waveform properties showed that only T_0 appeared to be elongated when the circuit was equipped with *Msg5* loop. The significance of the difference between conditions was assessed with two-sample Student's t tests. (n.s., not significant; **p < 0.01).

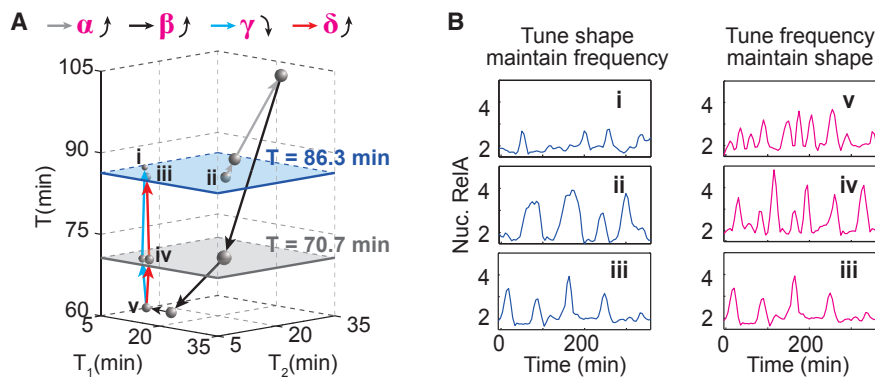


Figure 7. Custom Design of Oscillatory Signaling Dynamics

(A) Design space diagram of the sequential tuning of the synthetic oscillatory signaling circuit. Each oscillatory waveform was characterized by four properties: T_1 , T_2 , T (period), and A (amplitude, indicated by ball radii). The arrows represent the changes in oscillatory waveforms in response to the tuning of aforementioned circuit parameters or circuit topology: α (light gray), β (dark gray), γ (blue), and δ (pink). Two groups of oscillation waveforms identified in two iso-period planes (conditions in such a plane share the same frequency: blue, $T = 86.3$ min; gray, $T = 70.7$ min) have different peak shape properties.

(B) Representative single-cell trajectories in (A) show that engineered oscillatory dynamics could be tuned in both peak shape-only and frequency-only manner.

the oscillation of the activated RelA behaved less robustly nevertheless (Figure S6C).

DISCUSSION

In this work, we synthetically engineered an oscillatory signaling circuit via rewiring the human NF- κ B module within the yeast mating MAPK pathway. This system enabled us to systematically explore how the quantitative properties of the output waveforms were determined by either circuit parameters or circuit structures. Our engineered circuit was capable of generating as wide a range of behaviors as has been observed in similar, naturally occurring circuits (Elowitz and Lim, 2010; O’Shaughnessy et al., 2011). Our findings provide a framework for using a synthetic approach to study intricate natural biological systems, and demonstrate that biological oscillatory signaling dynamics can be quantitatively and predictably designed (Kiel et al., 2010; Lim, 2010).

The difference in the oscillation pattern observed between the native and synthetic circuits highlights an advantage of the orthogonality of our synthetic system, which ostensibly experiences much less cross-reactivity due to the lack of additional components of the native system that have been suggested to be responsible for the damping effect (Hoffmann et al., 2002; Werner et al., 2008). A previous study, for instance, has suggested that the A20-mediated negative feedback loop might function as a “rheostat” and control the decay of NF- κ B oscillation in response to TNF- α (Werner et al., 2008). The addition of a second negative feedback regulation layer (mediated by Msg5) to our synthetic NF- κ B circuit nevertheless clearly demonstrates a unique circuit structure that enables frequency modulation of signaling outputs. In this case, Msg5 functions as a “frequency modulator” instead of a “rheostat.” Frequency modulation in diverse organisms has long been recognized (Berridge, 1997; Levine et al., 2013). The oscillatory frequency, moreover, has been known as a high order of regulatory factor by which cells coordinate their responses to varied signal dosages (Cai et al., 2008). More recently, it was discovered that multiple pulsatile waveforms interacted combinatorially to control downstream gene transcription (Lin et al., 2015), highlighting the importance of further investigating the underlying

principles of more complex oscillatory dynamics tuning in natural signaling systems.

Our synthetic NF- κ B circuit also represents an efficient way to engineer robust oscillatory signaling circuit in eukaryotic cells, with no requirement for additional controls such as positive feedbacks or carefully selected parameter sets (Potvin-Trottier et al., 2016; Stricker et al., 2008; Tsai et al., 2008). The robust oscillation of our synthetic circuit suggested that the sequestering mechanism of I κ B α -RelA complex introduced sufficient ultrasensitivity to the activation of RelA, and contributed to the oscillation robustness magnificently (Buchler and Cross, 2009). Meanwhile, the regulation in subcellular localization of RelA might introduce extra nonlinearity and effective time delay. The core module of our design, formed by a pre-inhibited transcriptional factor (RelA) and an inhibitory protein (I κ B α), represented a general molecular architecture for inducible activation. Such a design could be applied to any other signaling circuits sharing similar molecular architectures. Notably, the activation of a transcription factor can be easily wired to downstream transcriptional circuits and therefore control specific cell functions.

From the evolutionary perspective, our tuning results suggest that oscillatory signaling patterns could easily evolve in a core circuit design such as NF- κ B; it also suggests that the behavior of the natural NF- κ B system is quite plastic. For example, evolutionary modification in either the amino acid motifs that regulate protein stability, or in DNA elements of promoters that control feedback and constant expression of circuit components, could lead to rapidly evolving patterns of activation dynamics.

The orthogonality and simplicity of the synthetic circuit promoted the accuracy of computational modeling, and facilitated the experimental validation of predicted functions. The refined modeling results could improve our capability of implementing theory-guided precise dynamic perturbation, as well as *de novo* design of oscillatory signaling circuits. Our findings demonstrated that the oscillatory dynamics can be designed with customized peak shape or frequency in a predictive manner. The design of a specific made-to-order oscillatory waveform may require strategies for modulating individual waveform properties, such as the amplitude, frequency, rest

time, etc. For example, in certain scenario, one might require either specific tuning of the peak shape without changing the period, or tuning of the period without changing the peak shape. Our data have shown that these properties can be custom designed by synthetically manipulating the underlying circuit parameters and circuit structures, or in combination (Figures 7A and 7B). In practice, such tuning of circuit parameters or structures could also be controlled by additional cellular signals. By doing so, a single signaling circuit is capable of encoding multiplex dynamics (Levine et al., 2013; Purvis and Lahav, 2013). This suggests that synthetic oscillatory signaling circuits could be an ideal model system to explore further challenging questions, such as how the signaling dynamics are decoded by downstream transcriptional regulation. Notably, our synthetic circuit encodes cellular inputs at both the transcriptional and the post-translational level (e.g., phosphorylation, ubiquitination), suggesting that diverse upstream signaling dynamics may be investigated.

We suggest that in future, oscillatory circuit designs are likely to be utilized in many applications that require the precise coordination of multiple sub-functional engineered circuits. For instance, a circuit could be engineered into synthetic therapeutic cells to encode an oscillatory control program that can interpret multiplexed inputs including antigens, cytokines, or stress levels. The cell can therefore sense the proximity to the tumor niche, and respond appropriately via the control circuit with stimulus-specific commands, for either cytotoxic functions to kill tumor or safety-switch function to suicide. In many other cases such as metabolic engineering, this central processor can introduce an oscillatory timing control of production of targeted chemicals, so as to minimize the toxicity caused by the unwanted accumulated intermediates, or to maximize the final production by optimizing the ratio of precursors. In short, increasingly complex devices in synthetic biology will necessarily require increasingly sophisticated designs for their information control system, our oscillatory dynamics-tunable signaling circuit being a functioning prototype of it.

STAR★METHODS

Detailed methods are provided in the online version of this paper and include the following:

- **KEY RESOURCES TABLE**
- **CONTACT FOR REAGENT AND RESOURCE SHARING**
- **EXPERIMENTAL MODEL AND SUBJECT DETAILS**
- **METHOD DETAILS**
 - Plasmids and Strains Construction
 - Flow Cytometry Experiments
 - Microfluidics and Fluorescent Microscopy
 - Image Processing
 - Mathematical Model
- **QUANTIFICATION AND STATISTICAL ANALYSIS**
 - RelA Protein Concentration, Promoter Strength and κ B α Degradation Rate
 - Single-Cell RelA-GFP Localization Dynamics and Waveform Properties
 - Statistical Analysis
- **DATA AND SOFTWARE AVAILABILITY**

SUPPLEMENTAL INFORMATION

Supplemental Information includes six figures, three tables, and five movies and can be found with this article online at <https://doi.org/10.1016/j.cels.2017.09.016>.

AUTHOR CONTRIBUTIONS

P.W. conceived the project. P.W. and Z.Z. designed the experiments. Z.Z., Q.W., Y.K., S.L., J.J., and P.W. performed the experiments and analyzed the data. Z.Z., C.T., and P.W. performed the computational modeling. Z.Z., W.A.L., and P.W. wrote the manuscript.

ACKNOWLEDGMENTS

This work was supported by the National Key Basic Research Program of China 2015CB910300 (P.W.), the National Natural Science Foundation of China 31470819 (P.W.), 31622022 (P.W.), and 91430217 (C.T.).

Received: June 8, 2017

Revised: July 18, 2017

Accepted: September 25, 2017

Published: October 25, 2017

SUPPORTING CITATIONS

The following references appear in the Supplemental Information: Maeder et al. (2007).

REFERENCES

- Ashall, L., Horton, C.A., Nelson, D.E., Paszek, P., Harper, C.V., Sillitoe, K., Ryan, S., Spiller, D.G., Unitt, J.F., and Broomhead, D.S. (2009). Pulsatile stimulation determines timing and specificity of NF- κ B-dependent transcription. *Science* 324, 242–246.
- Bashor, C.J., Helman, N.C., Yan, S., and Lim, W.A. (2008). Using engineered scaffold interactions to reshape MAP kinase pathway signaling dynamics. *Science* 319, 1539–1543.
- Behar, M., and Hoffmann, A. (2010). Understanding the temporal codes of intra-cellular signals. *Curr. Opin. Genet. Dev.* 20, 684–693.
- Berridge, M.J. (1997). The AM and FM of calcium signalling. *Nature* 386, 759–760.
- Buchler, N.E., and Cross, F.R. (2009). Protein sequestration generates a flexible ultrasensitive response in a genetic network. *Mol. Syst. Biol.* 5, 272.
- Cai, L., Dalal, C.K., and Elowitz, M.B. (2008). Frequency-modulated nuclear localization bursts coordinate gene regulation. *Nature* 455, 485–490.
- Elowitz, M., and Lim, W.A. (2010). Build life to understand it. *Nature* 468, 889–890.
- Elowitz, M.B., and Leibler, S. (2000). A synthetic oscillatory network of transcriptional regulators. *Nature* 403, 335–338.
- Ferrell, J.E., Jr., Tsai, T.Y., and Yang, Q. (2011). Modeling the cell cycle: why do certain circuits oscillate? *Cell* 144, 874–885.
- Gilmore, T.D., and Wolenski, F.S. (2012). NF- κ B: where did it come from and why? *Immunol. Rev.* 246, 14–35.
- Gordley, R.M., Williams, R.E., Bashor, C.J., Toettcher, J.E., Yan, S., and Lim, W.A. (2016). Engineering dynamical control of cell fate switching using synthetic phospho-regulons. *Proc. Natl. Acad. Sci. USA* 113, 13528–13533.
- Hao, N., Budnik, B.A., Gunawardena, J., and O'Shea, E.K. (2013). Tunable signal processing through modular control of transcription factor translocation. *Science* 339, 460–464.
- Hasty, J., Dolnik, M., Rottschäfer, V., and Collins, J.J. (2002). Synthetic gene network for entraining and amplifying cellular oscillations. *Phys. Rev. Lett.* 88, 148101.
- Hayden, M.S., and Ghosh, S. (2008). Shared principles in NF- κ B signaling. *Cell* 132, 344–362.

- Hess, B., and Boiteux, A. (1971). Oscillatory phenomena in biochemistry. *Annu. Rev. Biochem.* *40*, 237–258.
- Hoffmann, A., Levchenko, A., Scott, M.L., and Baltimore, D. (2002). The I κ B-NF- κ B signaling module: temporal control and selective gene activation. *Science* *298*, 1241–1245.
- Kachroo, A.H., Laurent, J.M., Yellman, C.M., Meyer, A.G., Wilke, C.O., and Marcotte, E.M. (2015). Evolution. Systematic humanization of yeast genes reveals conserved functions and genetic modularity. *Science* *348*, 921–925.
- Kiel, C., Yus, E., and Serrano, L. (2010). Engineering signal transduction pathways. *Cell* *140*, 33–47.
- Levine, J.H., Lin, Y., and Elowitz, M.B. (2013). Functional roles of pulsing in genetic circuits. *Science* *342*, 1193–1200.
- Lim, W.A. (2010). Designing customized cell signalling circuits. *Nat. Rev. Mol. Cell Biol.* *11*, 393–403.
- Lin, Y., Sohn, C.H., Dalal, C.K., Cai, L., and Elowitz, M.B. (2015). Combinatorial gene regulation by modulation of relative pulse timing. *Nature* *527*, 54–58.
- Maeder, C.I., Hink, M.A., Kinkhabwala, A., Mayr, R., Bastiaens, P.I.H., and Knop, M. (2007). Spatial regulation of Fus3 MAP kinase activity through a reaction-diffusion mechanism in yeast pheromone signalling. *Nat. Cell Biol.* *9*, 1319–1326.
- McClung, C.R. (2008). Comes a time. *Curr. Opin. Plant Biol.* *11*, 514–520.
- Mengel, B., Krishna, S., Jensen, M.H., and Trusina, A. (2012). Nested feedback loops in gene regulation. *Phys. Stat. Mech. Appl.* *391*, 100–106.
- Mondragon-Palomino, O., Danino, T., Selimkhanov, J., Tsimring, L., and Hasty, J. (2011). Entrainment of a population of synthetic genetic oscillators. *Science* *333*, 1315–1319.
- Nelson, D., Ihekwaba, A., Elliott, M., Johnson, J., Gibney, C., Foreman, B., Nelson, G., See, V., Horton, C., and Spiller, D. (2004). Oscillations in NF- κ B signaling control the dynamics of gene expression. *Science* *306*, 704–708.
- Novák, B., and Tyson, J.J. (2008). Design principles of biochemical oscillators. *Nat. Rev. Mol. Cell Biol.* *9*, 981–991.
- O'Shaughnessy, E.C., Palani, S., Collins, J.J., and Sarkar, C.A. (2011). Tunable signal processing in synthetic MAP kinase cascades. *Cell* *144*, 119–131.
- Oates, A.C., Morelli, L.G., and Ares, S. (2012). Patterning embryos with oscillations: structure, function and dynamics of the vertebrate segmentation clock. *Development* *139*, 625–639.
- Partch, C.L., Green, C.B., and Takahashi, J.S. (2014). Molecular architecture of the mammalian circadian clock. *Trends Cell Biol.* *24*, 90–99.
- Peisajovich, S.G., Garbarino, J.E., Wei, P., and Lim, W.A. (2010). Rapid diversification of cell signaling phenotypes by modular domain recombination. *Science* *328*, 368–372.
- Potvin-Trottier, L., Lord, N.D., Vinnicombe, G., and Paulsson, J. (2016). Synchronous long-term oscillations in a synthetic gene circuit. *Nature* *538*, 514–517.
- Purvis, J.E., Karhohs, K.W., Mock, C., Batchelor, E., Loewer, A., and Lahav, G. (2012). p53 dynamics control cell fate. *Science* *336*, 1440–1444.
- Purvis, J.E., and Lahav, G. (2013). Encoding and decoding cellular information through signaling dynamics. *Cell* *152*, 945–956.
- Stricker, J., Cookson, S., Bennett, M.R., Mather, W.H., Tsimring, L.S., and Hasty, J. (2008). A fast, robust and tunable synthetic gene oscillator. *Nature* *456*, 516–519.
- Tay, S., Hughey, J.J., Lee, T.K., Lipniacki, T., Quake, S.R., and Covert, M.W. (2010). Single-cell NF- κ B dynamics reveal digital activation and analogue information processing. *Nature* *466*, 267–271.
- Tsai, T.Y.-C., Choi, Y.S., Ma, W., Pomeroy, J.R., Tang, C., and Ferrell, J.E. (2008). Robust, tunable biological oscillations from interlinked positive and negative feedback loops. *Science* *321*, 126–129.
- Tyson, J.J. (1991). Modeling the cell division cycle: cdc2 and cyclin interactions. *Proc. Natl. Acad. Sci. USA* *88*, 7328–7332.
- Werner, S.L., Barken, D., and Hoffmann, A. (2005). Stimulus specificity of gene expression programs determined by temporal control of IKK activity. *Science* *309*, 1857–1861.
- Werner, S.L., Kearns, J.D., Zadorozhnaya, V., Lynch, C., O'Dea, E., Boldin, M.P., Ma, A., Baltimore, D., and Hoffmann, A. (2008). Encoding NF- κ B temporal control in response to TNF: distinct roles for the negative regulators I κ B α and A20. *Genes Dev.* *22*, 2093–2101.
- Yang, X., Lau, K.Y., Sevim, V., and Tang, C. (2013). Design principles of the yeast G1/S switch. *PLoS Biol.* *11*, e1001673.
- Zambrano, S., Bianchi, M.E., and Agresti, A. (2014). High-throughput analysis of NF- κ B dynamics in single cells reveals basal nuclear localization of NF- κ B and spontaneous activation of oscillations. *PLoS One* *9*, e90104.

STAR★METHODS

KEY RESOURCES TABLE

REAGENT or RESOURCE	SOURCE	IDENTIFIER
Chemicals, Peptides, and Recombinant Proteins		
LB Broth	BD	240210
ssDNA	Invitrogen	15632-011
EDTA	Amresco	E0105
Sodium chloride	Sigma-Aldrich	S5886
Ampicillin	Amresco	0339
Agar	BD	214510
Yeast nitrogen base without amino acids	BD	291920
Dextrose Glucose Anhydrous	BD	215510
Adenine hemisulfate salt	Sigma-Aldrich	A3159
Glycine	Sigma-Aldrich	50046
L-Alanine	Sigma-Aldrich	A7627
L-Arginine	Sigma-Aldrich	A5006
L-Asparagine	Sigma-Aldrich	A0884
L-Aspartic acid	Sigma-Aldrich	A7219
L-Cysteine	Sigma-Aldrich	168149
L-Glutamine	Sigma-Aldrich	G3126
L-Glutamic acid monosodium salt hydrate	Sigma-Aldrich	G1626
L-Histidine	Sigma-Aldrich	H8000
L-Isoleucine	Sigma-Aldrich	I7403
L-Leucine	Sigma-Aldrich	L8000
L-Lysine	Sigma-Aldrich	L8662
L-Methionine	Sigma-Aldrich	M5308
L-Phenylalanine	Sigma-Aldrich	P2126
L-Proline	Sigma-Aldrich	P5607
L-Serine	Sigma-Aldrich	S4500
L-Threonine	Sigma-Aldrich	T8441
L-Tryptophan	Sigma-Aldrich	T8941
L-Tyrosine	Sigma-Aldrich	T8566
L-Valine	Sigma-Aldrich	V0513
myo-Inositol	Sigma-Aldrich	I5125
para-Aminobenzoic Acid	Sigma-Aldrich	A9878
Uracil	Sigma-Aldrich	U0750
Cycloheximide	Sigma-Aldrich	C1988
α -factor	GenScript	RP01002
Doxycycline hyclate	Sigma-Aldrich	D9181
Hygromycin B	Thermo Fisher Scientific	10687010
Concanavalin A	Sigma-Aldrich	C2010
Poly(ethylene glycol)	Sigma-Aldrich	P4338
Lithium acetate	Sigma-Aldrich	517992
Critical Commercial Assays		
AarI restriction enzyme	Thermo Fisher Scientific	ER1581
PmeI restriction enzyme	NEB	R0560L
T4 DNA Ligase	NEB	M0202L
KOD-Plus-Neo	TOYOBO	KOD-401

(Continued on next page)

Continued		
REAGENT or RESOURCE	SOURCE	IDENTIFIER
TIANprep Midi Plasmid Kit	TIANGEN	DP106
Universal DNA Purification Kit	TIANGEN	DP124
2×Taq PCR MasterMix	TIANGEN	KT201
ZeroBack Fast Ligation Kit	TIANGEN	VT204
Experimental Models: Organisms/Strains		
See Table S1 for a full list of yeast strains for this study	This paper	N/A
Recombinant DNA		
See Table S2 for a full list of plasmids for this study	This paper	N/A
Software and Algorithms		
Matlab code to analyze single-cell RelA-GFP time series data	This paper	https://github.com/ZhangZhibo87/2017-Cell-Zhang
Matlab	MathWorks	https://www.mathworks.com/
ImageJ	NIH	https://imagej.nih.gov/ij/
FlowJo	FlowJo, LLC	https://www.flowjo.com/
Other		
CellASIC Y04D microfluidic plates	EMD Millipore	Y04C-02-5PK
CellASIC ONIX microfluidic platform	EMD Millipore	EV262

CONTACT FOR REAGENT AND RESOURCE SHARING

Further information and requests for resources and reagents should be directed to and will be fulfilled by the Lead Contact, Ping Wei (pwei@pku.edu.cn).

EXPERIMENTAL MODEL AND SUBJECT DETAILS

All yeast strains used in this study and the figures where each strain is used are listed in [Table S1](#). Unless otherwise specified, the parent yeast strain for all our synthetic strains was CB008 (*W303 MATa far1 his3 trp1 leu2 ura3*). The deletion of *FAR1* gene allowed the cells to response to α -factor stimulation without arresting their cell cycle. The growth conditions are described as below.

METHOD DETAILS

Plasmids and Strains Construction

All plasmids used in this study ([Table S2](#)) were constructed by using a method for alternative assembly based on the Type IIIs restriction enzyme AarI ([Peisajovich et al., 2010](#)). The human genes RelA and I κ B α were cloned from human cDNA (Invitrogen). The basic NF- κ B-inducible promoter was constructed by fusing four repeats of a 10bp- κ B binding site upstream to a minimal yeast CYC1 promoter. The other promoter variants with different levels of transcriptional activity were engineered with the similar strategy. Yeast transformations were done with the standard LiAc method. The engineered genetic components were integrated in a single copy into the genome through a set of integrating yeast vectors (*pNH603*, *pNH604*, *pNH605*, *pNH606*, *pNH607*). All yeast genomic integrations were confirmed by yeast colony PCR.

Flow Cytometry Experiments

Analysis of circuit parameters, i.e., the concentration of RelA, the transcriptional activity of our engineered promoters, the degradation rate of degron-tagged I κ B α , and the inhibitory efficiency of the negative regulator Msg5, were performed by measuring fluorescent protein (GFP or mCherry) intensity with a Becton Dickinson LSRiI flow cytometer (high throughput sampler equipped). For all FACS experiments, triplicate cultures were grown in synthetic complete dropout media at 30°C to early log phase (OD600 = 0.1-0.2). To tune the concentration of RelA protein in the cells, we used a doxycycline-regulated system to control expression of GPF-RelA protein. 100 μ L aliquots was taken at time = 0 and after 2 hours of induction of variant concentrations of doxycycline (Sigma-Aldrich). In the experiments to survey promoters, 5 μ g/mL doxycycline were added into each separate culture at time = 0. 100 μ L aliquots was taken at time = 0 and after 2 hours of induction to measure the intensity of a fluorescent reporter (mCherry). To trace the degradation of mCherry-I κ B α , we measured the time courses of fluorescent intensity in corresponding strains after adding the stimulation of 10 μ M α -factor (GenScript). 100 μ L aliquots was taken at each time point. In the experiments to test Msg5, a mating pathway-dependent reporter was constructed by fusing the promoter *pFUS1* with GFP in the parent strain

CB008. 100 μ L aliquots was taken at time = 0 and after 3 hours of 10 μ M α -factor treatment. All sampled aliquots were treated with 5 μ g/mL cycloheximide (Sigma-Aldrich) before flow cytometer measurements. 10,000 cells were counted for each reading.

Microfluidics and Fluorescent Microscopy

The microfluidic cell cultures were performed in Y04C yeast perfusion plates with an ONIX flow control system (Millipore). Cultures were grown in synthetic complete dropout media to mid-log phase (OD600 = 0.2-0.8). Before loading cells, the flow chamber was pre-coated with concanavalin A. Once loaded, cells were flowed over by synthetic complete dropout media for more than 30 min before applying α -factor or doxycycline stimulation. Image acquisition was performed with a TE2000-E automated inverted microscope (Nikon) with perfect focus system and a 100 \times oil immersion lens.

Image Processing

We monitored the dynamic behaviors of our synthetic signaling circuit by live single-cell fluorescent microscopy. Based on bright field images, cell segmentation and tracing were done automatically by customized Matlab software cellseg (Yang et al., 2013). The backgrounds of all fluorescence images were first subtracted by ImageJ (1.49v, Java1.6.0_24, 64-bit). The single-cell dynamics data, such as that mCherry-I κ B α degradation and RelA-GFP nuclear localization, was then extracted from these processed time-lapsed fluorescence images also by cellseg.

Mathematical Model

The dynamics of the synthetic system was modeled by ordinary differential equations (ODEs), which was mainly based on a previous work (Ashall et al., 2009) describing the NF- κ B system in mammalian cells. In contrast to the original model, we made three modifications: (1) for quantifying the degradation rate of free I κ B α and I κ B α in complex with RelA, we simplified the two-step process of phosphorylation and degradation, by a single Michaelis-Menten function; (2) for the process of protein synthesis, mRNA nuclear export was considered to get enough time delay; (3) for Msg5 feedback module, the concentration of phosphorylated Fus3 was directly regulated by Msg5 protein.

$$pFus3 = \max(0, pFus3_{\max} - 0.0001 \times Msg5^2)$$

$$\frac{d}{dt} nRelA(t) = kv \times kimpr \times RelA(t) - kv \times kexpr \times nRelA(t) - ka \times nI\kappa B\alpha(t) \times nRelA(t) + kd \times nRelA|I\kappa B\alpha(t) + dpc \times nRelA|I\kappa B\alpha(t)$$

$$\begin{aligned} \frac{d}{dt} RelA(t) = & pFus3 \times Vm \times \frac{RelA|I\kappa B\alpha(t)}{RelA|I\kappa B\alpha(t) + Km} - kimpr \times RelA(t) + kexpr \times nRelA(t) - ka \times I\kappa B\alpha(t) \\ & \times RelA(t) + kd \times RelA|I\kappa B\alpha(t) + dpc \times RelA|I\kappa B\alpha(t) \end{aligned}$$

$$\frac{d}{dt} nI\kappa B\alpha(t) = kv \times kimp_i \times I\kappa B\alpha(t) - kv \times kexp_i \times nI\kappa B\alpha(t) - ka \times nI\kappa B\alpha(t) \times nRelA(t) + kd \times nRelA|I\kappa B\alpha(t) - dp \times nI\kappa B\alpha(t)$$

$$\begin{aligned} \frac{d}{dt} I\kappa B\alpha(t) = & -pFus3 \times Vm \times \frac{I\kappa B\alpha(t)}{I\kappa B\alpha(t) + Km} - kimp_i \times I\kappa B\alpha(t) + kexp_i \times nI\kappa B\alpha(t) + kt \times TrI\kappa B\alpha(t) - ka \times I\kappa B\alpha(t) \\ & \times RelA(t) + kd \times RelA|I\kappa B\alpha(t) - dp \times I\kappa B\alpha(t) \end{aligned}$$

$$\frac{d}{dt} nTrI\kappa B\alpha(t) = Vh \times \frac{nRelA^h(t)}{nRelA^h(t) + Kh^h} - dt \times nTrI\kappa B\alpha(t) - kv \times kexp_t \times nTrI\kappa B\alpha(t)$$

$$\frac{d}{dt} TrI\kappa B\alpha(t) = k \exp t \times nTrI\kappa B\alpha(t) - dt \times TrI\kappa B\alpha(t)$$

$$\frac{d}{dt} nRelA|IkB\alpha(t) = kv \times kimpc \times RelA|IkB\alpha(t) - kv \times kexpc \times nRelA|IkB\alpha(t) + ka \times nIkB\alpha(t) \times nRelA(t) - kd \times nRelA|IkB\alpha(t) - dpc \times nRelA|IkB\alpha(t)$$

$$\frac{d}{dt} RelA|IkB\alpha(t) = -pFus3 \times Vm \times \frac{RelA|IkB\alpha(t)}{RelA|IkB\alpha(t) + Km} - kimpc \times RelA|IkB\alpha(t) + kexpc \times nRelA|IkB\alpha(t) + ka \times IkB\alpha(t) \times RelA(t) - kd \times RelA|IkB\alpha(t) - dpc \times RelA|IkB\alpha(t)$$

$$\frac{d}{dt} nTrMsg5(t) = Vhm \times \frac{nRelA^h(t)}{nRelA^h(t) + Kh^h} - dt \times nTrMsg5(t) - kv \times kexpt \times nTrMsg5(t)$$

$$\frac{d}{dt} TrMsg5(t) = kexpt \times nTrMsg5(t) - dt \times TrMsg5(t)$$

$$\frac{d}{dt} Msg5(t) = kt \times TrMsg5(t) - dpm \times Msg5(t)$$

All the variables were quantified by their molar concentration. Messenger RNA transcripts were denoted by Tr . The $IkB\alpha$ -RelA complex was denoted by $RelA|IkB\alpha$. The letter n indicated nuclear localization, while the cytoplasmic localization was omitted. Transport rates for nuclear molecular species were adjusted by the ratio of cytoplasmic to nuclear volumes (kv), to account for different compartmental volumes.

The activity of feedback promoters was calibrated based on the expression levels of their downstream fluorescent protein. Specifically, measured fluorescent levels of all promoters (Fp , Figure 3B) were first normalized by that of $pNFkB059$ and then mapped into promoter activity (Vh) by an affine transformation: $Vh = ah \times norm.Fp + bh$ ($norm.Fp$ equals parameter β in text; $ah = 0.0023 \text{ nM} \cdot \text{s}^{-1}$, $bh = 0.011 \text{ nM} \cdot \text{s}^{-1}$, obtained by globally fitting). Similarly, the concentration of initial cytoplasmic RelA (initial cR) was calibrated by initial $cR = ar \times norm.Fr + br$ (Fr represented RelA-GFP levels in Figure 3A, the value in the condition of $5 \mu\text{g/mL}$ doxycycline was normalized as 1, and $norm.Fr$ equals parameter γ in text; $ar = 1500 \text{ nM}$, $br = 1000 \text{ nM}$, obtained by globally fitting). While for the degradation rate of $IkB\alpha$ via degron (Vm), we first calculated the slope (Sl) of the line which went through the first two time points in mCherry- $IkB\alpha$ dynamics (Figure 3C) for each degron and then normalized them by WT's slope. Vm was calibrated by the equation $Vm = am \times norm.Sl + bm$ ($norm.Sl$ equals parameter α in text; $am = 0.0047 \text{ s}^{-1}$, $bm = -0.0017 \text{ s}^{-1}$, also obtained by globally fitting).

Besides the three experimentally turned parameters (Vh , initial cR and Vm), the other ones were retained from literature values or refined accounting for the differences between mammalian cells and yeast cells (Table S3). In the case of simulating single-feedback circuit, we set Vhm as 0. For the parallel feedbacks, a second negative regulator, $IkBx$, was added to the present model. $IkB\alpha$ and $IkBx$ shared almost all characteristics, except for the transcription rate and degradation rate via degron.

All the variables were initialized to be 0, except for cytoplasmic RelA, the amount of which is set as 2500 nM in the conditions of $5 \mu\text{g/mL}$ doxycycline. Our simulations were initiated with maximum phosphorylated Fus3 concentration ($pFus3max$) equal to zero. After equalizing for 20 hours, maximum phosphorylated Fus3 ($pFus3max$) was raised to 600 nM by a step function (refer to addition of α -factor, Figure 4B).

QUANTIFICATION AND STATISTICAL ANALYSIS

RelA Protein Concentration, Promoter Strength and $IkB\alpha$ Degradation Rate

We used a doxycycline-inducible promoter $pTET07$ to tune the level of RelA-GFP protein and measured its stable concentration by flow cytometry at three gradient doses of doxycycline (i.e. 0.5, 1, and $5 \mu\text{g/mL}$, see Figure 3A). To assess the transcriptional activities of our engineered RelA-inducible promoters (Figure 3B) and yeast native constitutive promoters (Figure S6A), we measured the expression of a fluorescent reporter (mCherry) under consistent conditions as previously described in Flow Cytometry Experiments of METHOD DETAILS. To quantify the degradation rate of $IkB\alpha$ via variant engineered degrons, we tagged mCherry at their N-terminal and recorded the time courses of fluorescent intensities after α -factor stimulation. Degradation rate of each degron got assigned the value of the straight-line slope by fitting the first two data points in its corresponding time course.

Single-Cell RelA-GFP Localization Dynamics and Waveform Properties

Within the boundary of one cell, we quantified the average intensity of the brightest 10×10 RelA-GFP pixels as nuclear RelA-GFP concentration, and quantified the average intensity of the all pixels as total RelA-GFP concentration. To indicate the subcellular localization of RelA protein, we used the nuclear to total ratio of the RelA-GFP concentration which was denoted as Nuc. RelA. The time series of single-cell Nuc.RelA was acquired automatically by customized Matlab programs. Each single-cell trajectory was smoothed by a Savitzky-Golay filter of degree 2 before further analysis.

Oscillatory waveform properties including period and peak shape characteristics were analyzed by a custom-made Matlab program for peak detection in single-cell Nuc.RelA trajectories. The core algorithm adopted a work previously developed to find significant peaks in time courses of mammalian NF- κ B dynamics and discard fluctuations due to noise (Zambrano et al., 2014). Specifically, a peak was defined as a sequence of a left local minimum, a central local maximum and a right local minimum. Based on detected peaks, period equaled to the time lags between successive central maximums, rise time equaled to the time lags between the left minimum and its following central maximum, decay time equaled to the time lags between the central maximum and its following right minimum, rest time equaled to the right minimum and its following left minimum and the amplitude equaled to the difference between the Nuc.RelA signals at the central maximum and a pre-set threshold. We analyzed all of our RelA-GFP dynamics data automatically under the same set of parameters, including amplitude pre-set threshold and minimal peak number. For every single measurement, 50-100 cells were collected to calculate periods and other waveform characteristics. On average, we can acquire 3~5 peak-distances from each single cell trajectory (for each measurement, > 150 peak-distance in total). We then calculated the mean of all peak-distances as the oscillation period for that experiment. The four waveform properties were analyzed following the similar protocol.

Statistical Analysis

Statistical parameters were reported in the Figures and Figure Legends. All statistical analysis was performed in Matlab R2014a (MathWorks).

DATA AND SOFTWARE AVAILABILITY

The five files used for demonstrating how we detect peaks in single-cell Nuc.RelA time series data and calculate waveform properties are found on https://github.com/ZhangZhibo87/2017-Cell_Systems-Zhang. Therein, “ipeaksNarrow.m” is used to detect notable peaks with rational boundaries in single-cell Nuc.RelA time series data and “WaveformProperties.m” is a function to identify oscillatory period and the other four waveform characteristics (i.e., rest time, rise time, decay time and amplitude).

Cell Systems, Volume 5

Supplemental Information

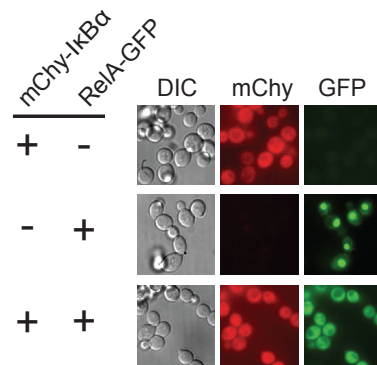
Design of Tunable Oscillatory Dynamics in a Synthetic NF- κ B Signaling Circuit

Zhi-Bo Zhang, Qiu-Yue Wang, Yu-Xi Ke, Shi-Yu Liu, Jian-Qi Ju, Wendell A. Lim, Chao Tang, and Ping Wei

Supplemental Figures

A

Subcellular localization of human RelA and I κ B α in yeast cells



B

Cytosolic Cdc4 (NES-Cdc4)-dependent degradation of degron-tagged I κ B α

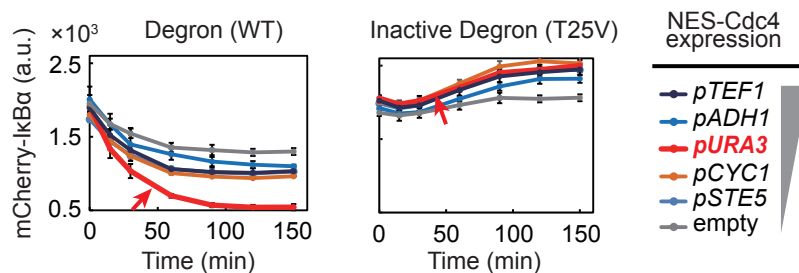


Figure S1. The Design Diagram of a Functional Synthetic NF- κ B Circuit in the Budding Yeast, Related to Figure 1

(A) Subcellular localizations of fluorescent protein-tagged I κ B α and RelA in yeast cells. mCherry-I κ B α localized to the cytoplasm and RelA-GFP localized to the nucleus when expressed respectively. In contrast, when both proteins were co-expressed, RelA-GFP and mCherry-I κ B α co-localized to the cytoplasm.

(B) Mating signaling-stimulated degradation of engineered I κ B α depends on the cytosolic yeast E3 ligase Cdc4. The degradation of mCherry-I κ B α tagged with wild type degron (left panel) or inactive mutant degron (right panel, T25V) were measured by flow cytometer with or without cytosolic Cdc4. The wild type Cdc4 was tagged with nuclear export signal (NES), and driven by a set of yeast constitutive promoters (from strongest to weakest: *pTEF1* (dark), *pADH1* (blue), *pURA3* (red, bold), *pCYC1* (orange), *pSTE5* (light blue), or empty plasmid (grey)). 10 μ M α -factor was added at time zero to initiate the phosphorylation and degradation of mCherry-I κ B α -degron. *pURA3* (highlighted by red arrow) was selected as the optimal promoter to express NES-Cdc4 in most of the experiments in the main text. The standard deviation of three experimental repeats were calculated as error bars.

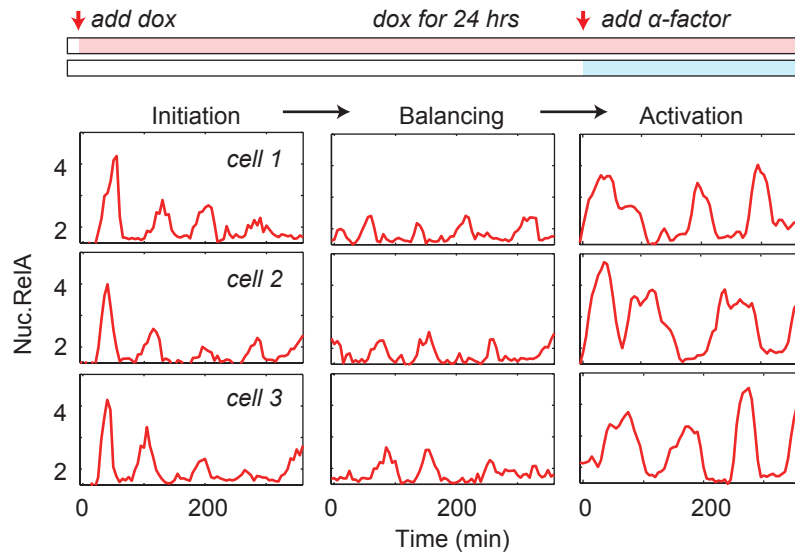


Figure S2. Mating pheromone-activated Periodic RelA Nuclear Translocation, Related to Figure 2

The single-cell dynamics of RelA-GFP nuclear translocation in yeast cells engineered with the synthetic signaling circuit was recorded. The circuit was stimulated at time zero by adding 5 $\mu\text{g}/\text{mL}$ doxycycline to induce RelA-GFP expression (*pTET07_RelA-GFP*). The early induced RelA-GFP first freely translocated into the nucleus (no I κ B α yet) and then were translocated out of nucleus after the RelA-induced I κ B α -degron expression (*pNF κ B_I κ B α -degron*). After 24 hour-balancing with continuous treatment of doxycycline, RelA-GFP was still spontaneously but weakly pulsing even in absence of α -factor. When stimulated with 10 μM α -factor, cells were activated and oscillated robustly.

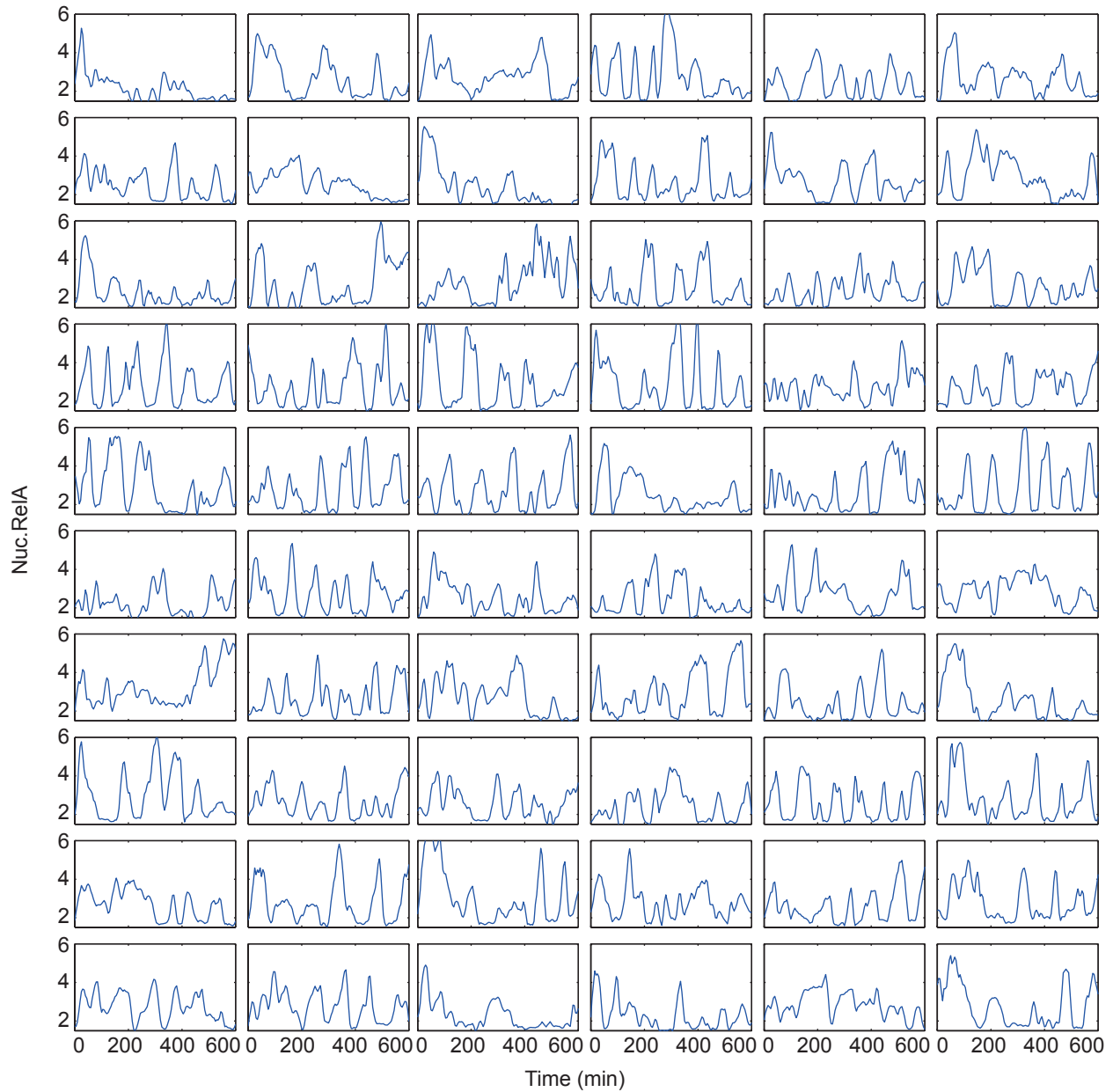


Figure S3. Single-cell Trajectories of RelA-GFP Nuclear Translocation after α -factor stimulation, Related to Figure 2
 Yeast cells engineered with the synthetic signaling oscillator was continuously cultured in 5 $\mu\text{g}/\text{mL}$ doxycycline for over 12 hours and then activated by 10 μM α -factor at time zero. The ratio of nuclear to total RelA-GFP was calculated to indicate the RelA activation dynamics. Over 50 cells were recorded in each experiment.

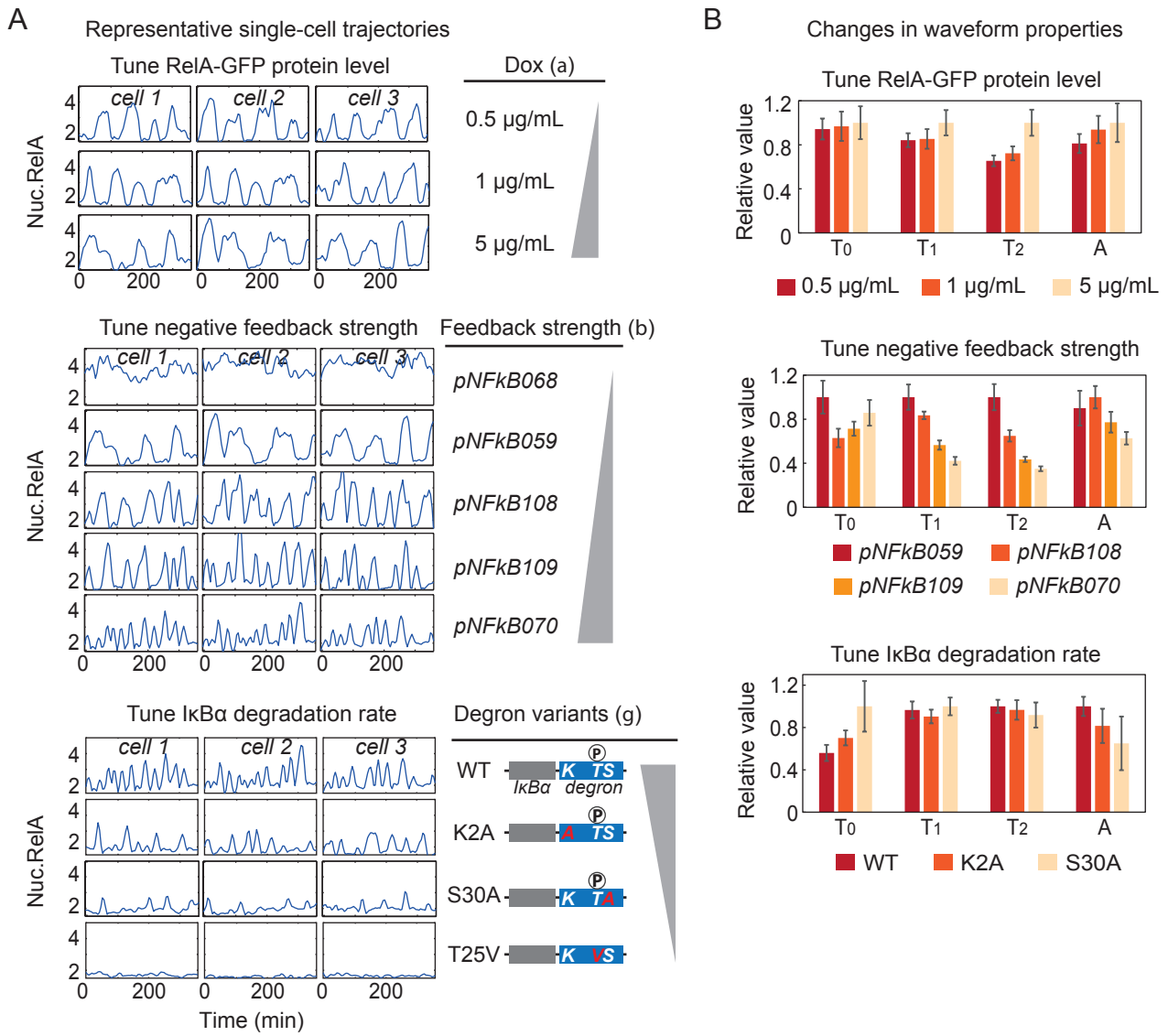


Figure S4. Systematically Tuning Circuit Parameters and Quantitatively Characterizing Oscillatory Waveforms, Related to Figure 3

(A) Representative single-cell dynamics of RelA activation were recorded when tuning the three parameters.

(B) Changes in the waveform properties after parameter-tuning. Each properties were normalized to the maximum value. Error bars represented the standard deviation from at least three repeated experiments.

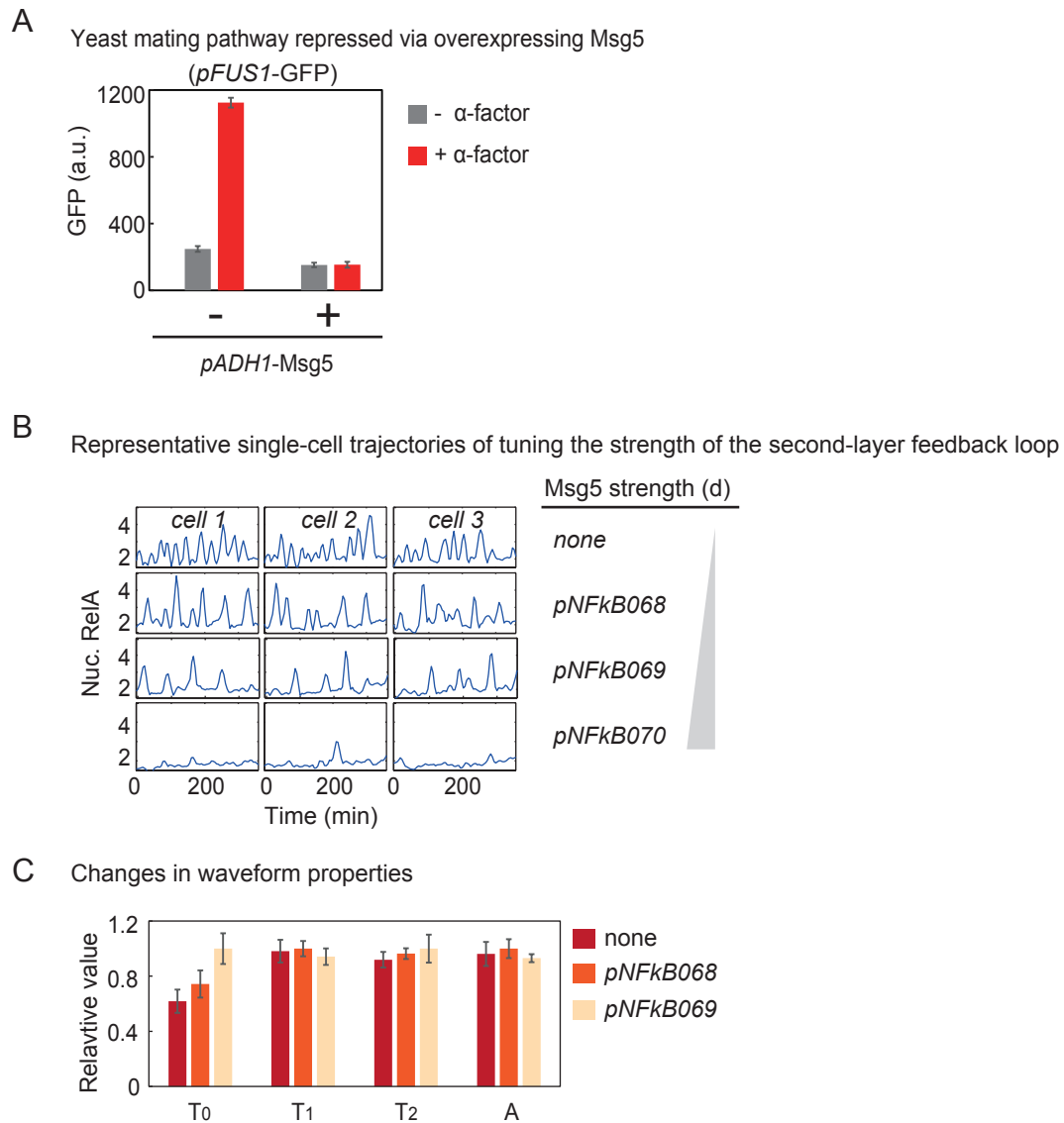


Figure S5. Experimentally Tuning the Second Layer of Negative Feedback Loop via Msg5 Enables Frequency-only Tuning of the Waveforms without Changing the Peak Shape, Related to Figure 5

(A) The repressive activity of yeast MAPK phosphatase Msg5 in yeast mating response was indicated by GFP level driven by a mating-specific promoter *pFUS1* (measured by flow cytometer). Msg5 was over-expressed by *pADH1* promoter. Error bars represented the standard deviation from triplicated experiments.

(B) Representative single-cell dynamics of RelA activation were recorded when gradually tuning the strength of the second layer of negative feedback loop.

(C) Only T_0 was changed in the waveform properties by tuning Msg5 feedback strength. The maximum value of each properties was normalized as "1". Error bars represented the standard deviation from at least three repeated experiments.

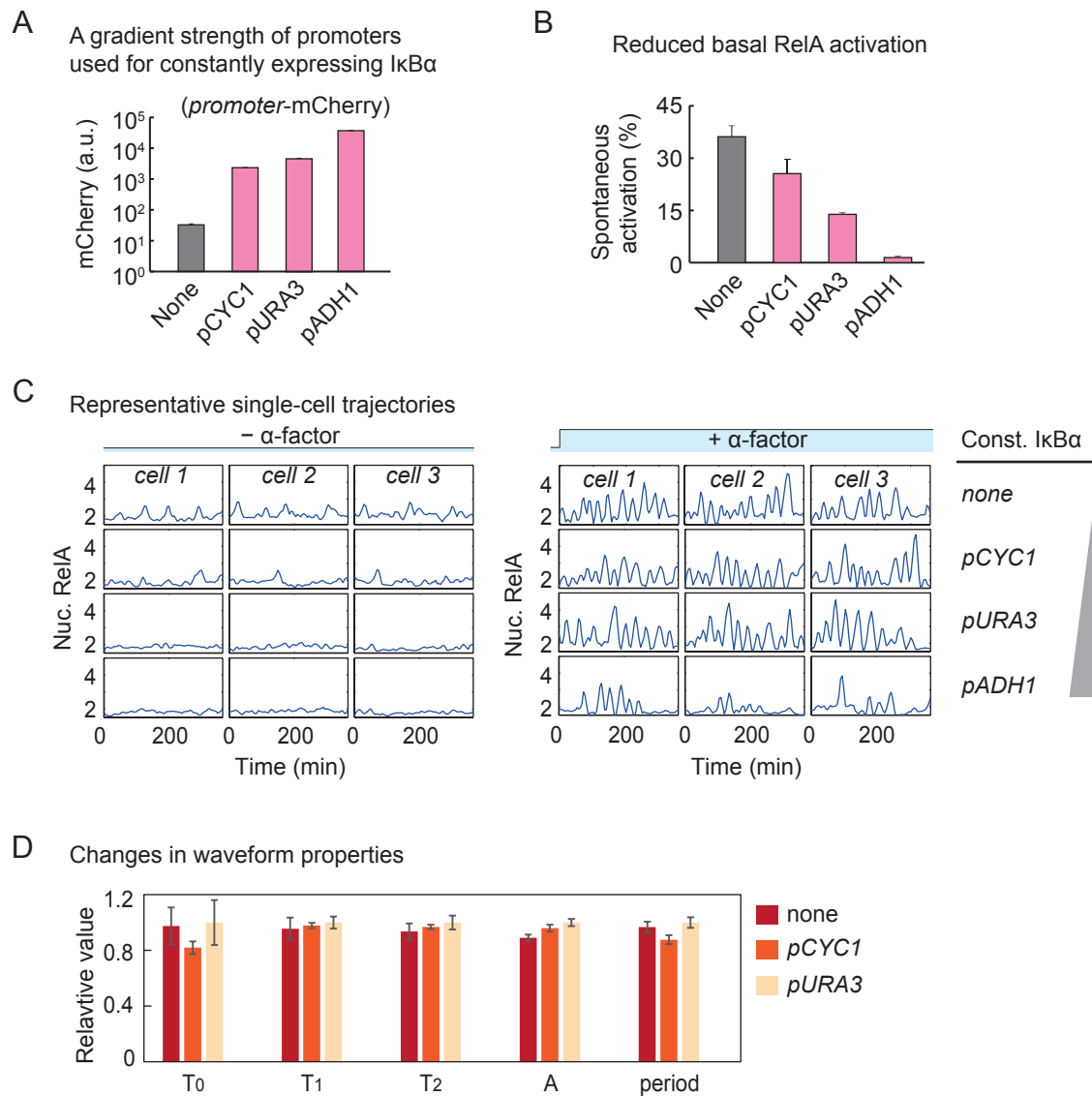


Figure S6. Adding Constantly-expressed IκBα Effectively Reduced the Spontaneous RelA Activation without Changing the Waveform Properties, Related to Figure 6

(A) The mCherry expression level driven by a set of constitutive yeast promoters. These promoters were then used to tune the level of constantly-expressed IκBα.

(B) Statistical analysis of the spontaneously activated cells in absence of α-factor stimulation. The increased protein level of constantly-expressed IκBα reduced the basal RelA activation. The spontaneous activation was calculated from the percentage of activated cell. A cell, in which RelA nuclear translocation shows at least one detectable peak within a 6 hour-window without α-factor, was considered as the activated cell. At least 50 cells were included in each experiment.

(C) Representative single-cell dynamics of RelA activation were recorded when tuning the expression of constant IκBα. When the constantly-expressed IκBα reached in very high level, the α-factor triggered oscillation was also diminished.

(D) The waveform properties remain unchanged when adding the constantly-expressed IκBα. The maximum value of each properties was normalized as “1”.

(A, B, and D) Error bars represented the standard deviation from triplicated experiments.

SUPPLEMENTARY TABLES

Table S1. Yeast Strains Used in This Study. Related to STAR Methods.

Strain	Genotype	Figure it is used in
scZBZ006	<i>W303 MATa, far1Δ, pADH1-rtTA::HygB, pTET07-3×Flag-RelA-GFP::LEU2, pURA3-NES-Cdc4::HIS3, pTEF1-mCherry-IκBα-WTDegron::TRP1, ura3</i>	1D; 3C; S1A
scZBZ007	<i>W303 MATa, far1Δ, pADH1-rtTA::HygB, pTET07-3×Flag-RelA-GFP::LEU2, pURA3-NES-Cdc4::HIS3, pTEF1-mCherry-IκBα-T25VDegron::TRP1, ura3</i>	3C
scZBZ012	<i>W303 MATa, far1Δ, pADH1-rtTA::HygB, pTET07-3×Flag-RelA-GFP::LEU2, pURA3-NES-Cdc4::HIS3, trp1, ura3</i>	S1A; S6A
scZBZ029	<i>W303 MATa, far1Δ, pADH1-rtTA::HygB, pTET07-3×Flag-RelA-GFP::LEU2, pURA3-NES-Cdc4::HIS3, pNFkB059-1×Flag-IκBα-WTDegron::URA3, trp1</i>	2A,B,D; 3A,D,E; 7; S2; S3; S4
scZBZ034	<i>W303 MATa, far1Δ, pADH1-rtTA::HygB, pTET07-3×Flag-RelA-GFP::LEU2, pURA3-NES-Cdc4::HIS3, pTEF1-mCherry-IκBα-WTDegron::TRP1, pNFkB059-GFP::URA3</i>	1D
scZBZ035	<i>W303 MATa, far1Δ, pADH1-rtTA::HygB, pTET07-3×Flag-RelA-GFP::LEU2, pURA3-NES-Cdc4::HIS3, pTEF1-mCherry-IκBα-T25VDegron::TRP1, pNFkB059-GFP::URA3</i>	1D
scZBZ055	<i>W303 MATa, far1Δ, pADH1-rtTA::HygB, pTET07-3×Flag-RelA-GFP::LEU2, pURA3-NES-Cdc4::HIS3, pNFkB070-1×Flag-IκBα-WTDegron::URA3, trp1</i>	3E,F; 5C-F; 6B-D S4D; S5B,C S6B-D
scZBZ069	<i>W303 MATa, far1Δ, pADH1-rtTA::HygB, pTET07-3×Flag-RelA-GFP::LEU2, pURA3-NES-Cdc4::HIS3, pNFkB068-1×Flag-IκBα-WTDegron::URA3, trp1</i>	S4A
scZBZ088	<i>W303 MATa, far1Δ, pADH1-rtTA::HygB, pTET07-3×Flag-RelA-GFP::LEU2, pURA3-NES-Cdc4::HIS3, pTEF1-mCherry-IκBα-K2ADegron::TRP1, ura3</i>	3A
scZBZ093	<i>W303 MATa, far1Δ, pADH1-rtTA::HygB, pTET07-3×Flag-</i>	3A

	<i>RelA-GFP::LEU2, pURA3-NES-Cdc4::HIS3, pTEF1-mCherry-IκBα-S30ADegron::TRP1, ura3</i>	
scZBZ097	<i>W303 MATa, far1Δ, pADH1-rtTA::HygB, pTET07-3×Flag-RelA-GFP::LEU2, pURA3-NES-Cdc4::HIS3, pNFκB070-1×Flag-IκBα-WTDegron::URA3, pURA3-1×Flag-IκBα-WTDegron::TRP1</i>	6B-D; S6B-D
scZBZ098	<i>W303 MATa, far1Δ, pADH1-rtTA::HygB, pTET07-3×Flag-RelA-GFP::LEU2, pURA3-NES-Cdc4::HIS3, pNFκB070-1×Flag-IκBα-WTDegron::URA3, pADH1-1×Flag-IκBα-WTDegron::TRP1</i>	S6B,C
scZBZ101	<i>W303 MATa, far1Δ, pADH1-rtTA::HygB, pTET07-3×Flag-RelA-GFP::LEU2, pURA3-NES-Cdc4::HIS3, pNFκB070-1×Flag-IκBα-K2ADegron::URA3, trp1</i>	3F; 7A; S4
scZBZ102	<i>W303 MATa, far1Δ, pADH1-rtTA::HygB, pTET07-3×Flag-RelA-GFP::LEU2, pURA3-NES-Cdc4::HIS3, pNFκB070-1×Flag-IκBα-S30ADegron::URA3, trp1</i>	3F; 7; S4
scZBZ106	<i>W303 MATa, far1Δ, pADH1-rtTA::HygB, pTET07-3×Flag-RelA-GFP::LEU2, pURA3-NES-Cdc4::HIS3, pNFκB070-1×Flag-IκBα-T25VDegron::URA3, trp1</i>	S4A
scZBZ122	<i>W303 MATa, far1Δ, pADH1-rtTA::HygB, pTET07-3×Flag-RelA-GFP::LEU2, pURA3-NES-Cdc4::HIS3, pNFκB108-1×Flag-IκBα-WTDegron::URA3, trp1</i>	3E; 7A; S4
scZBZ123	<i>W303 MATa, far1Δ, pADH1-rtTA::HygB, pTET07-3×Flag-RelA-GFP::LEU2, pURA3-NES-Cdc4::HIS3, pNFκB109-1×Flag-IκBα-WTDegron::URA3, trp1</i>	3E; 7A; S4
scZBZ151	<i>W303 MATa, far1Δ, pADH1-rtTA::HygB, pTET07-3×Flag-RelA-GFP::LEU2, pURA3-NES-Cdc4::HIS3, pNFκB059-1×Flag-mCherry::URA3, trp1</i>	3B
scZBZ152	<i>W303 MATa, far1Δ, pADH1-rtTA::HygB, pTET07-3×Flag-RelA-GFP::LEU2, pURA3-NES-Cdc4::HIS3, pNFκB068-1×Flag-mCherry::URA3, trp1</i>	3B
scZBZ153	<i>W303 MATa, far1Δ, pADH1-rtTA::HygB, pTET07-3×Flag-RelA-GFP::LEU2, pURA3-NES-Cdc4::HIS3, pNFκB069-1×Flag-mCherry::URA3, trp1</i>	3B
scZBZ154	<i>W303 MATa, far1Δ, pADH1-rtTA::HygB, pTET07-3×Flag-RelA-GFP::LEU2, pURA3-NES-Cdc4::HIS3, pNFκB070-</i>	3B

	<i>1</i> ×Flag-mCherry::URA3, <i>trp1</i>	
scZBZ156	<i>W303 MATa, far1Δ, pADH1-rtTA::HygB, pTET07-3</i> ×Flag-RelA-GFP::LEU2, <i>pURA3-NES-Cdc4::HIS3, pNFkB108-1</i> ×Flag-mCherry::URA3, <i>trp1</i>	3B
scZBZ157	<i>W303 MATa, far1Δ, pADH1-rtTA::HygB, pTET07-3</i> ×Flag-RelA-GFP::LEU2, <i>pURA3-NES-Cdc4::HIS3, pNFkB109-1</i> ×Flag-mCherry::URA3, <i>trp1</i>	3B
scZBZ169	<i>W303 MATa, far1Δ, pADH1-rtTA::HygB, pTET07-3</i> ×Flag-RelA-GFP::LEU2, <i>pURA3-NES-Cdc4::HIS3, pURA3-1</i> ×Flag-mCherry::TRP1, <i>ura3</i>	S6A
scZBZ171	<i>W303 MATa, far1Δ, pADH1-rtTA::HygB, pTET07-3</i> ×Flag-RelA-GFP::LEU2, <i>pURA3-NES-Cdc4::HIS3, pADH1-1</i> ×Flag-mCherry::TRP1, <i>ura3</i>	S6A
scZBZ183	<i>W303 MATa, far1Δ, pADH1-rtTA::HygB, pTET07-3</i> ×Flag-RelA-GFP::LEU2, <i>pTEF1-mCherry-IκBα-WTDegron::TRP1, pSTE5-NES-Cdc4::HIS3, trp1</i>	S1B
scZBZ184	<i>W303 MATa, far1Δ, pADH1-rtTA::HygB, pTET07-3</i> ×Flag-RelA-GFP::LEU2, <i>pTEF1-mCherry-IκBα-WTDegron::TRP1, pCYC1-NES-Cdc4::HIS3, trp1</i>	S1B
scZBZ185	<i>W303 MATa, far1Δ, pADH1-rtTA::HygB, pTET07-3</i> ×Flag-RelA-GFP::LEU2, <i>pTEF1-mCherry-IκBα-WTDegron::TRP1, pADH1-NES-Cdc4::HIS3, trp1</i>	S1B
scZBZ186	<i>W303 MATa, far1Δ, pADH1-rtTA::HygB, pTET07-3</i> ×Flag-RelA-GFP::LEU2, <i>pTEF1-mCherry-IκBα-WTDegron::TRP1, pURA3-NES-Cdc4::HIS3, trp1</i>	S1B
scZBZ187	<i>W303 MATa, far1Δ, pADH1-rtTA::HygB, pTET07-3</i> ×Flag-RelA-GFP::LEU2, <i>pTEF1-mCherry-IκBα-WTDegron::TRP1, pTEF1-NES-Cdc4::HIS3, trp1</i>	S1B
scZBZ188	<i>W303 MATa, far1Δ, pADH1-rtTA::HygB, pTET07-3</i> ×Flag-RelA-GFP::LEU2, <i>pTEF1-mCherry-IκBα-T25VDegron::TRP1, pSTE5-NES-Cdc4::HIS3, trp1</i>	S1B
scZBZ189	<i>W303 MATa, far1Δ, pADH1-rtTA::HygB, pTET07-3</i> ×Flag-RelA-GFP::LEU2, <i>pTEF1-mCherry-IκBα-T25VDegron::TRP1, pCYC1-NES-Cdc4::HIS3, trp1</i>	S1B
scZBZ190	<i>W303 MATa, far1Δ, pADH1-rtTA::HygB, pTET07-3</i> ×Flag-RelA-GFP::LEU2, <i>pTEF1-mCherry-IκBα-</i>	S1B

	<i>T25VDegron::TRP1, pADH1-NES-Cdc4::HIS3, trp1</i>	
scZBZ191	<i>W303 MATa, far1Δ, pADH1-rtTA::HygB, pTET07-3×Flag-RelA-GFP::LEU2, pTEF1-mCherry-IκBα-T25VDegron::TRP1, pURA3-NES-Cdc4::HIS3, trp1</i>	S1B
scZBZ192	<i>W303 MATa, far1Δ, pADH1-rtTA::HygB, pTET07-3×Flag-RelA-GFP::LEU2, pTEF1-mCherry-IκBα-T25VDegron::TRP1, pTEF1-NES-Cdc4::HIS3, trp1</i>	S1B
scZBZ235	<i>W303 MATa, far1Δ, pADH1-rtTA::HygB, pTET07-3×Flag-RelA-GFP::LEU2, pURA3-NES-Cdc4::HIS3, pNFkB059-1×Flag-IκBα-WTDegron::URA3, pNFkB068-Msg5::TRP1</i>	7; S5B,C
scZBZ237	<i>W303 MATa, far1Δ, pADH1-rtTA::HygB, pTET07-3×Flag-RelA-GFP::LEU2, pURA3-NES-Cdc4::HIS3, pNFkB059-1×Flag-IκBα-WTDegron::URA3, pNFkB069-Msg5::TRP1</i>	5C-F; 7; S5B,C
scZBZ239	<i>W303 MATa, far1Δ, pADH1-rtTA::HygB, pTET07-3×Flag-RelA-GFP::LEU2, pURA3-NES-Cdc4::HIS3, pNFkB059-1×Flag-IκBα-WTDegron::URA3, pNFkB070-Msg5::TRP1</i>	S5B
scZBZ240	<i>W303 MATa, far1Δ, bar1Δ, pFUS1-GFP::MFA2, pADH1-Msg5::LEU2, his3, trp1, ura3</i>	S5A
scZBZ246	<i>W303 MATa, far1Δ, pADH1-rtTA::HygB, pTET07-3×Flag-RelA-GFP::LEU2, pURA3-NES-Cdc4::HIS3, pNFkB070-1×Flag-IκBα-WTDegron::URA3, pCYC1-1×Flag-IκBα-WTDegron::TRP1</i>	S6B-D
scZBZ249	<i>W303 MATa, far1Δ, pADH1-rtTA::HygB, pTET07-3×Flag-RelA-GFP::LEU2, pURA3-NES-Cdc4::HIS3, pCYC1-1×Flag-mCherry::TRP1, ura3</i>	S6A
CB009	<i>W303 MATa, far1Δ, bar1Δ, pFUS1-GFP::MFA2, his3, trp1, leu2, ura3</i>	S5A

Table S2. Plasmids Used in This Study. Related to STAR Methods.

Plasmid	Parent vector / Selection	Promoter	Gene
pWP412	pNH607(HygB)	pADH1	rtTA
pWP466	pNH605(LEU)	pTET07	3×Flag-RelA-mCerulean
pWP471	pNH604(TRP)	pTEF1	mCherry-IκBα-WTDegron
pWP472	pNH604(TRP)	pTEF1	mCherry-IκBα-T25VDegron
pWP476	pNH606(URA)	pNFκB059	GFP
pWP477	pNH605(LEU)	pTET07	3×Flag-RelA-GFP
pZBZ001	pNH603(HIS)	pURA3	NES-Cdc4
pZBZ015	pNH606(URA)	pNFκB059	1×Flag-IκBα-WTDegron
pZBZ033	pNH603(HIS)	pSTE5	NES-Cdc4
pZBZ034	pNH603(HIS)	pCYC1	NES-Cdc4
pZBZ035	pNH603(HIS)	pADH1	NES-Cdc4
pZBZ036	pNH603(HIS)	pTEF1	NES-Cdc4
pZBZ043	pNH606(URA)	pNFκB068	1×Flag-IκBα-WTDegron
pZBZ048	pNH606(URA)	pNFκB070	1×Flag-IκBα-WTDegron
pZBZ053	pNH604(TRP)	pURA3	1×Flag-IκBα-WTDegron
pZBZ054	pNH604(TRP)	pCYC1	1×Flag-IκBα-WTDegron
pZBZ059	pNH606(URA)	pNFκB059	1×Flag-mCherry
pZBZ063	pNH604(TRP)	pADH1	1×Flag-IκBα-WTDegron
pZBZ068	pNH606(URA)	pNFκB068	1×Flag-mCherry
pZBZ069	pNH606(URA)	pNFκB069	1×Flag-mCherry
pZBZ070	pNH606(URA)	pNFκB070	1×Flag-mCherry
pZBZ073	pNH604(TRP)	pTEF1	mCherry-IκBα-K2ADegron

pZBZ078	pNH604(TRP)	pTEF1	mCherry-I κ B α -S30ADegron
pZBZ080	pNH606(URA)	pNF κ B070	1 \times Flag-I κ B α -K2ADegron
pZBZ081	pNH606(URA)	pNF κ B070	1 \times Flag-I κ B α -S30ADegron
pZBZ097	pNH606(URA)	pNF κ B070	1 \times Flag-I κ B α -T25VDegron
pZBZ099	pNH606(URA)	pNF κ B108	1 \times Flag-I κ B α -WTDegron
pZBZ100	pNH606(URA)	pNF κ B109	1 \times Flag-I κ B α -WTDegron
pZBZ108	pNH606(URA)	pNF κ B108	1 \times Flag-mCherry
pZBZ109	pNH606(URA)	pNF κ B109	1 \times Flag-mCherry
pZBZ112	pNH604(TRP)	pURA3	1 \times Flag-mCherry
pZBZ114	pNH604(TRP)	pADH1	1 \times Flag-mCherry
pZBZ157	pNH604(TRP)	pNF κ B068	Msg5
pZBZ158	pNH604(TRP)	pNF κ B069	Msg5
pZBZ159	pNH604(TRP)	pNF κ B070	Msg5
pZBZ163	pNH605(LEU)	pADH1	Msg5
pZBZ191	pNH604(TRP)	pCYC1	1 \times Flag-mCherry

Table S3. Parameters Used in the Mathematical Model. Related to STAR Methods.

Symbol	Description	Value	References
<i>kv</i>	Ratio of cytoplasmic to nuclear volume	9	Measured
<i>ka</i>	RelA-I κ B α complex formation rate	0.0005 nM ⁻¹ ·s ⁻¹	Hoffmann et al., 2002
<i>kd</i>	RelA-I κ B α complex dissociation rate	0.0005 s ⁻¹	Hoffmann et al., 2002
<i>kimpi</i>	I κ B α nuclear import	0.0007 s ⁻¹	Ashall et al., 2009
<i>kexpi</i>	I κ B α nuclear export	0.0007 s ⁻¹	Assumption
<i>kimpr</i>	RelA nuclear import	0.0006 s ⁻¹	2×ki1 in Ashall et al., 2009
<i>kexpr</i>	RelA nuclear export	0.000012 s ⁻¹	Ashall et al., 2009, kimpr/50
<i>kimpc</i>	RelA-I κ B α nuclear import	0.0002 s ⁻¹	Assumption kexpc/100
<i>kexpc</i>	RelA-I κ B α nuclear export	0.02 s ⁻¹	2×ke2a in Ashall et al., 2009
<i>kexpt</i>	I κ B α transcript nuclear export	0.00025 s ⁻¹	Assumption
<i>Vh</i>	Maximum transcription rate of I κ B α	0.0123 nM·s ⁻¹ for <i>pNFkB059</i> promoter	Fitted
<i>h</i>	Hill coefficient	3	Fitted
<i>Kh</i>	Half-max constant in Hill function	500	Fitted
<i>kt</i>	Translation rate	3 s ⁻¹	Assumption
<i>Vm</i>	Maximum degradation rate via degron	0.003 s ⁻¹ for WT Degron	Fitted
<i>Km</i>	Half-max constant in Michaelis-Menten function	700	Fitted
<i>dt</i>	mRNA transcripts degradation rate	0.0012 s ⁻¹	Half-life~10 min

<i>dp</i>	Free I κ B α degradation rate	0.001 s ⁻¹	Half-life~12 min
<i>dpc</i>	I κ B α complexed with RelA degradation rate	0.00004 s ⁻¹	Hoffmann et al., 2002
<i>pFus3max</i>	Maximal concentration of phosphorylated Fus3 kinase	0 nM (no α -factor)/ 600 nM (add 10 μ M α -factor)	Maeder et al., 2007
<i>Vhm</i>	Maximum transcription rate of Msg5	Same as <i>Vm</i>	Fitted
<i>dpm</i>	Msg5 degradation rate	0.003 s ⁻¹	Half-life~4 min